Earth and Planetary Science Letters 362 (2013) 51–65

Contents lists available at SciVerse ScienceDirect

Earth and Planetary Science Letters

journal homepage: www.elsevier.com/locate/epsl

The climate of the Late Cretaceous: New insights from the application of the carbonate clumped isotope thermometer to Western Interior Seaway macrofossil

K.J. Dennis [a,*], J.K. Cochran [b], N.H. Landman [c], D.P. Schrag [a]

[a] Department of Earth and Planetary Sciences, Harvard University, 20 Oxford Street, Cambridge, MA 02318, USA
[b] School of Marine and Atmospheric Sciences, Stony Brook University, Stony Brook, NY 11794, USA
[c] Division of Paleontology, American Museum of Natural History, Central Park West at 79th Street, New York, NY 10024, USA

ARTICLE INFO

Article history:
Received 8 May 2012
Received in revised form
16 October 2012
Accepted 20 November 2012
Editor: G. Henderson

Keywords:
carbonate clumped isotope thermometry
Western Interior Seaway
Late Cretaceous
oxygen isotopes
disequilibrium precipitation
paleotemperature

ABSTRACT

We apply the carbonate clumped isotope thermometer (Δ_{47}) to macrofossils from the *Baculites compressus* (~73.5 Ma) and the *Hoploscaphites nebrascensis* (~67 Ma) ammonite zones of the Western Interior Seaway (WIS) of North America, and nearby coeval terrestrial and open marine environments. The carbonate clumped isotope thermometer is based on a single-phase isotope exchange equilibrium that promotes the 'clumping' of two heavy isotopes together within a single carbonate molecule as temperature decreases. Due to the thermometer's isotopic independence from water, coupled measurements of Δ_{47} and the bulk oxygen isotopic composition of a carbonate ($\delta^{18}O_c$) enable the reconstruction of both paleotemperature and the isotopic composition of the water in which the organisms grew. Before applying the technique to the aragonite shells of fossil marine organisms (mostly ammonites, but also some gastropods, bivalves, and one belemnite), we measure the clumped isotopic composition of modern nautilus and cuttlefish, two of the nearest living relatives to the Cretaceous ammonites. Modern cephalopods exhibit disequilibrium isotope effects with respect to Δ_{47}, but not $\delta^{18}O_c$, therefore a simple correctional scheme is applied to the Late Cretaceous macrofossil data before reconstructing paleotemperatures. Diagenesis is also assessed by visual preservation and previously measured Sr concentrations (Cochran et al., 2003). Temperatures reconstructed for the Late Cretaceous Western Interior Seaway range from 16.4 ± 3.5 °C for an offshore Interior Seaway environment from the *H. nebrascensis* zone to 24.2 ± 0.4 °C for the *B. compressus* ammonite zone. The seaway itself has an isotopic composition of approximately −1‰ (relative to VSMOW), the expectation for an ice-free global ocean average, while a nearby freshwater environment has an isotopic composition approaching −20‰. We compare the attributes of the reconstructed climate to predictions based on Late Cretaceous climate models and previous reconstructions of the seaway, and also assess the sensitivity of our results to the modern cephalopods correction by comparisons to suitable modern analogs. Finally, our clumped isotope data are consistent with cooling between the Late Campanian and Maastrichtian, as also seen in benthic foraminfera $\delta^{18}O$.

1. Introduction

Geochemical proxies (e.g., Barrera and Savin, 1999; Barron, 1983; Douglas and Savin, 1975; Huber et al., 2002), the geographic extent of climatically sensitive terrestrial and marine flora and fauna (Habicht, 1979; Markwick, 1998) and studies of leaf physiognomy (Davies-Vollum, 1997; Herman and Spicer, 1997) suggest the Cretaceous was a 'greenhouse' world marked by higher temperatures, a reduced equator-to-pole temperature gradient (Barron, 1983; Hay, 2008; Sloan and Barron, 1990) and elevated CO_2 concentrations (Arthur et al., 1985; Barron, 1985; Berner et al., 1983; Royer et al., 2001). A significant feature of the warmer world was the presence of large epicontinental seaways (Barron, 1983; Hancock and Kauffman, 1979), such as the Western Interior Seaway (WIS) of North America. At its greatest extent the WIS connected the boreal Arctic ocean with the Gulf of Mexico and covered the foreland basin of the western Cordillera (Miall et al., 2008) with seaway depths of about 200 m, with a possible maximum of 300 m (Hancock and Kauffman, 1979; McDonough and Cross, 1991). This sea level high coincided with the peak in Cretaceous greenhouse temperatures between about

* Corresponding author. Present address: Guyot Hall, Princeton University, Princeton, NJ 08544, USA. Tel.: +1 609 258 2756.
E-mail address: kdennis@princeton.edu (K.J. Dennis).

0012-821X/$ - see front matter © 2012 Elsevier B.V. All rights reserved.
http://dx.doi.org/10.1016/j.epsl.2012.11.036

100 to 85 Ma (Huber et al., 1995, 2002), after which global cooling proceeded until the end of the Cretaceous (Barrera and Savin, 1999; Clarke and Jenkyns, 1999; Huber et al., 1995, 2002). By the Late Campanian and Maastrichtian (from approximately 75–65 Ma), the WIS had receded significantly, was situated between 40° and 50°N, and had a maximum depth of about 100 m (Kauffman, 1984; Kennedy et al., 1998; Miall et al., 2008).

Reconstructing temperatures and paleoceanography, e.g., the circulation and connectivity to the open-ocean, of semi-enclosed epicontinental seaways can be challenging using traditional oxygen isotope paleothermometry. A primary reason for this is that the hydrological conditions of a seaway, e.g., local salinity and the oxygen isotopic composition of the water ($\delta^{18}O_w$), are difficult to constrain given their dependence on the balance of evaporation to precipitation and sources of freshwater. Assuming there is no long term change in the budget of oxygen isotopes in the hydrosphere, and for an ice-free world such as the Late Cretaceous, the global ocean average isotopic composition of seawater is expected to be about −1‰ on the VSMOW scale (Cramer et al., 2011; L'Homme, Clarke, 2005; Shackleton and Kennett, 1975), or −1.27‰ relative to the VPDB scale (Bemis et al., 1998; Hut, 1987; Shackleton and Kennett, 1975). Using this ice-free value, open-ocean paleotemperature reconstructions are possible given assumptions for meridional gradients in surface water $\delta^{18}O_w$ (e.g., Poulsen et al., 1999; Zachos et al., 1994). In contrast, the complex, and often unknown, hydrography and circulation of semi-enclosed basins make differentiating between changes in temperature and changes in $\delta^{18}O_w$ more difficult. This is especially important when sea level fluctuations are globally synchronous and forced by changes in ice volume, which will alter the isotopic composition of seawater temporally.

The carbonate clumped isotope thermometer is a valuable tool for reconstructing temperatures in such settings due to its independence from the isotopic composition of the water from which a carbonate precipitates. The thermometer is based on a single-phase, thermodynamically controlled, mass dependent isotope exchange reaction that orders ^{13}C and ^{18}O atoms into bonds with each other within a carbonate mineral lattice. As the formation temperature of the carbonate mineral decreases, the 'clumping' of these heavy isotopes into a single carbonate ion is promoted (Guo et al., 2009; Schauble et al., 2006; Wang et al., 2004). It is quantified using the parameter Δ_{47}, which measures the deviation in mass 47 CO_2 (mostly comprised of $^{13}C^{18}O^{16}O$, a 'clumped' isotopologue) from that expected given the sample's abundance of O and C isotopes, and it has an inverse relationship with temperature (Eiler, 2007; Eiler and Schauble, 2004; Wang et al., 2004). In the case of carbonate thermometry, the CO_2 is derived from acid digestion of a carbonate mineral, and Δ_{47} should reflect the temperature at which isotope exchange last occurred, likely in the carbonate or bicarbonate phase and at the water temperature at the time of mineral formation. Empirical calibrations using synthetic carbonates grown at controlled temperatures and modern natural carbonates have been shown to conform to the thermodynamic principle expected for clumped isotopologues of carbonate (Eiler, 2007, 2011; Ghosh et al., 2006, and the references therein), although some discrepancies between calibrations remain (Dennis et al., 2011; Dennis and Schrag, 2010), and some natural carbonates do not conform to synthetic carbonate calibrations (Affek et al., 2008; Daëron et al., 2011) suggesting disequilibrium isotope effects may be important for some carbonates.

Although the WIS has been studied in the past (e.g., Coulson et al., 2011; Slingerland et al., 1996), details about the paleotemperature and paleosalinity are difficult to infer using only oxygen and carbon isotopes in carbonates. For example, although assuming $\delta^{18}O_w = -1$‰ leads to reasonable temperature estimates for most cephalopods, other organisms, particularly inoceramid bivalves record temperatures in excess of 35 °C (Tourtelot and Rye, 1969). Explanations of these data have focused on either 'vital' effects[1] (Rye and Sommer, 1980; Tourtelot and Rye, 1969), or temperature and salinity stratification coupled to regional variability in the oxygen isotopic composition of the seaway (He et al., 2005; Wright, 1987). Unfortunately, these hypotheses cannot be tested without additional insight into the oxygen isotopic composition of the Seaway.

Another study by Cochran et al. (2003), examined the mixing of freshwater and seawater in the Maastrichtian WIS by measuring Sr isotopes in a variety of paleoenvironments. They found that the variation in $^{87}Sr/^{86}Sr$ between the open ocean and a brackish environment could not be explained by simple mixing between the freshwater and seawater end-members. Instead they hypothesized that submarine groundwater discharge could balance the Sr isotope budget, adding a further complexity to the hydrography of the Seaway. The successful application of clumped isotopes to the WIS would enhance our understanding of the temperature and $\delta^{18}O_w$ of the WIS, thereby improving our knowledge of (i) spatial variability in water properties, (ii) water column stratification, and (iii) the circulation of the Seaway.

By applying carbonate clumped isotope thermometry to a suite of macrofossils (also studied by Cochran et al., 2003), we seek to improve our understanding of paleosalinity and paleotemperature gradients in the Late Cretaceous WIS. Before doing so, we measure several modern shelled cephalopods, relatives of the Cretaceous ammonites, from known growth environments to assess if their $CaCO_3$ shells align with previous calibrations of the clumped isotope thermometer. Given evidence for disequilibrium precipitation, a correction is applied to the Late Cretaceous macrofossils before reconstructing temperatures and the isotopic composition of the shallow seaway. The climatic significance of our results is assessed by comparing them to (i) predictions based on Late Cretaceous climate models, (ii) previous reconstructions of the seaway and coeval terrestrial and open marine environments, and (iii) suitable analogs in the modern world. In addition, we compare our reconstructions from the Maastrichtian to the Late Campanian.

2. Materials and methods

2.1. Modern cephalopods

Modern cephalopods that grew at known temperatures were used to assess if their carbonate shells precipitated with the same dependence between temperature and Δ_{47} as synthetic carbonates (Table 1). Samples were loaned from the American Museum of Natural History (AMNH Loan number 512), the University of Tokyo via the AMNH (Loan number 509), and the Alfred Wegener Institute (AWI).

We selected to study modern nautilus because of their morphological similarities to Cretaceous ammonites, with both precipitating external, chambered shells. In addition, the chambered shell, which is comprised of aragonite, precipitates in oxygen isotopic equilibrium with water (Landman et al., 1994; Oba et al., 1992). Modern nautilus (*Nautilus pompilius, N. belauensis* and *N. macromphalus*) were either captured in the wild and moved to a temperature controlled aquarium (samples 1/8-6, 1/10-2, 1/10-3), raised in an aquarium (sample 89-39) or were wild for their entire lives (samples MN-1, AX and AR). The growth

[1] A vital effect is a generic term that reflects isotopic disequilibrium precipitation by an organism, possibly due to photosynthetic and/or metabolic activity (Epstein et al., 1951; Erez, 1978; Urey et al., 1951).

Table 1
Bulk and clumped isotope data for analysis of modern cephalopod aragonite. Growth temperatures are based on water temperatures profiles over ~150–400 m (New Caledonia and Bohol Strait Nautilus), prior studies (89-39, Landman et al., 1994), or provided by the laboratory that supplied the specimens (Kasai Aquarium Nautilus and Alfred Wegener Institute, AWI, aquarium Sepia). $\delta^{18}O_w$ is reported relative to VSMOW, and is compiled from local water column data (New Caledonia), aquarium measurements (Waikiki and AWI), or estimates of the local surface water $\delta^{18}O$ (Bohol Strait). $\delta^{13}C$ and $\delta^{18}O_c$ are reported relative to VPDB, and the errors are $\pm$ 0.04 and $\pm$ 0.05‰, respectively. The errors reported for Δ_{47} are the external standard error of the mean, except for samples only replicated two times, in which case it is the external standard deviation of the mean. The expected Δ_{47} value is calculated given the known growth temperature and the Δ_{47}-temperature calibration of Ghosh et al. (2006) (Eq. (3)). Also calculated is the difference between the expected Δ_{47} value and the measured Δ_{47} value, and the associated population 1σ standard deviation. If the oxygen isotopic composition of the water in which the organism grew is independently known, we assess if the shell precipitated in isotopic equilibrium. For the last column, the number in parentheses represents how close the sample is to isotopic equilibrium with respect to $\delta^{18}O_c$, i.e., within 1 or 2 °C. Sample names in bold text are those used to assess the average difference between expected Δ_{47} and measured Δ_{47}. Samples not included are either from a growth transect (samples 1/10-2-1 through 1/10-2-5), a cleaning test (samples followed by mc), or those that precipitated out of equilibrium with respect to $\delta^{18}O_c$.

Sample	Species	Growth environment	Growth T (°C)	$\delta^{18}O_w$ (‰)	n	$\delta^{13}C$ (‰)	$\delta^{18}O_c$ (‰)	Δ_{47} (‰)	Expected Δ_{47} (‰)	Difference	Equilibrium precipitation w.r.t. $\delta^{18}O_c$
Nautilus											
MN-1	*Nautilus macromphalus*	Wild—New Caledonia	16.4 ± 1.7	0.87 ± 0.2	2	−0.32	1.36	0.691 ± 0.014	0.754	0.063	Yes (2)
89-39	*Nautilus belauensis*	Waikiki Aquarium, Hawaii	22.2 ± 1.1	−0.2	2	−2.31	−0.44	0.663 ± 0.004	0.724	0.062	Yes (1)
1/8-6	*Nautilus pompilius*	Kasai Aquarium, Tokyo	21 ± 1	–	5	−3.02	0.54	0.671 ± 0.014	0.730	0.059	Unknown
1/10-2	*Nautilus pompilius*	Kasai Aquarium, Tokyo	21 ± 1	–	5	−2.84	0.43	0.662 ± 0.009	0.730	0.068	Unknown
1/10-2W	*Nautilus pompilius*	Wild—Bohol Strait	15 ± 2	0	4	−0.29	0.85	0.674 ± 0.003	0.761	0.087	Yes (1)
1/10-2S	*Nautilus pompilius*	Wild (final septa)—Bohol Strait	15 ± 2	0	4	−2.35	0.88	0.673 ± 0.011	0.761	0.089	Yes (1)
1/10-2J	*Nautilus pompilius*	Wild (juvenile)—Bohol Strait	23	0	3	0.10	−0.10	0.664 ± 0.009	0.720	0.056	Yes (2)
1/10-3	*Nautilus pompilius*	Kasai Aquarium, Tokyo	21 ± 1	–	5	−3.13	0.47	0.660 ± 0.009	0.730	0.071	Unknown
AX-juv	*Nautilus macromphalus*	Wild (juvenile)—New Caledonia	23	0.87 ± 0.2	4	0.35	0.38	0.670 ± 0.013	0.720	0.050	Yes (1)
AX-adu	*Nautilus macromphalus*	Wild (adult)—New Caledonia	16.4 ± 1.7	0.87 ± 0.2	3	1.23	1.60	0.671 ± 0.018	0.754	0.083	Yes (1)
AR-juv	*Nautilus macromphalus*	Wild (juvenile)—New Caledonia	23	0.87 ± 0.2	3	0.79	0.71	0.699 ± 0.018	0.720	0.022	Yes (2)
AR-adu	*Nautilus macromphalus*	Wild (adult)—New Caledonia	16.4 ± 1.7	0.87 ± 0.2	3	2.07	1.33	0.703 ± 0.014	0.754	0.051	Yes (2)
								Average difference		**0.063 ± 0.019**	
1/10-2-1	*Nautilus pompilius*	Wild—Bohol Strait	15 ± 2	0	3	0.92	0.95	0.696 ± 0.012	0.761	0.066	Yes (1)
1/10-2-2	*Nautilus pompilius*	Wild—Bohol Strait	15 ± 2	0	3	0.01	0.92	0.673 ± 0.007	0.761	0.088	Yes (1)
1/10-2-3	*Nautilus pompilius*	Wild—Bohol Strait	15 ± 2	0	3	0.28	1.05	0.662 ± 0.011	0.761	0.099	Yes (1)
1/10-2-4	*Nautilus pompilius*	Wild—Bohol Strait	15 ± 2	0	3	−0.63	0.92	0.695 ± 0.007	0.761	0.066	Yes (1)
1/10-2-5	*Nautilus pompilius*	Kasai Aquarium, Tokyo	21 ± 1	–	3	−2.71	0.77	0.676 ± 0.007	0.730	0.055	Unknown
1/10-2mc	*Nautilus pompilius*	Kasai Aquarium, Tokyo	21 ± 1	–	3	−2.83	0.73	0.667 ± 0.013	0.730	0.063	Unknown
1/10-3mc	*Nautilus pompilius*	Kasai Aquarium, Tokyo	21 ± 1	–	3	−2.91	0.60	0.660 ± 0.019	0.730	0.071	Unknown
Sepia											
K15Ch1	*Sepia officinalis*	Alfred Wegener Institute Aquarium, Bremerhaven	15	0	3	−2.32	1.07	0.711 ± 0.006	0.761	0.051	Yes (1)
K15Ch3	*Sepia officinalis*	Alfred Wegener Institute Aquarium, Bremerhaven	15	0	3	−1.99	1.50	0.725 ± 0.010	0.761	0.036	Yes (2)
K20Ch3	*Sepia officinalis*	Alfred Wegener Institute Aquarium, Bremerhaven		0	3	−2.91	0.10	0.699 ± 0.011	0.735	0.036	Yes (1)
K20Ch4	*Sepia officinalis*	Alfred Wegener Institute Aquarium, Bremerhaven	20	0	3	−2.75	−0.14	0.706 ± 0.012	0.735	0.030	Yes (2)
K15Ch2	*Sepia officinalis*	Alfred Wegener Institute Aquarium, Bremerhaven	15	0	4	−2.25	0.83	0.681 ± 0.007	0.761	0.080	Yes (2)
								Average difference		**0.047 ± 0.020**	
K15Ch5	*Sepia officinalis*	Alfred Wegener Institute Aquarium, Bremerhaven	15	0	4	−2.01	0.54	0.677 ± 0.010	0.761	0.085	No (3)
Nautilus and Sepia combined								**Average difference**		**0.059 ± 0.019**	

temperatures of nautilus were based on water temperatures profiles over ~150–400 m (New Caledonia and Bohol Strait nautilus; samples MN-1, AX, AR, 1/10-2 W, 1/10-2S, 1/10-2 J, and 1/10-2-1 to 1/10-2-4), prior studies (89-39, Landman et al., 1994), or provided by the laboratory that supplied the specimens (Kasai Aquarium nautilids; samples 1/8-6, 1/10-2, 1/10-3, 1/10-2-5, 1/10-2 mc, 1/10-3 mc). The isotopic composition of the water in which the specimens grew was also available for wild samples, based on local water column data (New Caledonia) or estimates of the local surface water $\delta^{18}O$ (Bohol Strait), and for the Waikiki aquarium-reared nautilus (Landman et al., 1994).

We also measured six specimens of *Sepia officinalis*, of the subclass Coleoidea. Although these cuttlefish are nektonic and precipitate aragonite, they have some important anatomical differences to the Cretaceous ammonites: modern cuttlefish precipitate internal skeletal carbonate (as did the ancient belemnites), while the ammonites and modern nautilus precipitate external shells (Clarkson, 1998). The *Sepia officinalis* specimens originate from the English Channel, but were reared under temperature controlled conditions at either 15 or 20 °C using North Sea water. Previous studies have reported that, as with the modern nautilus, cuttlefish precipitate skeletal carbonate in oxygen isotopic equilibrium with seawater (Rexfort and Mutterlose, 2006).

2.2. Cretaceous macrofossils

Late Cretaceous macrofossils from the WIS were loaned from AMNH (Loan number 503), the Yale Peabody Museum (Loan number 908) and the US National Museum, via AMNH (Loan number 503). The upper Cretaceous of the US Western Interior is subdivided into biostratigraphic zones and tied to radiometrically dated ash layers (Cobban et al., 2006) from the Lower Cenomanian (~100 Ma) to nearly the end of the Cretaceous in the Interior Seaway. Samples are from the *Baculites compressus* ammonite zone (~73.5 Ma) and the *Hoploscaphites nebrascensis* ammonite zone (~67 Ma), and were collected from the Pierre Shale, Fox Hills and Hell Creek Formations in South Dakota, and the Severn Formation in Maryland. Macrofossils from the *H. nebrascensis* zone are divided into paleoenvironmental groups (see Fig. 1 of Cochran et al., 2003) using the assessment of Waage (1968): 'Nearshore Interior' corresponds to nearshore facies within the seaway (Timber Lake Member of the Fox Hill Formation); 'Offshore Interior' corresponds to open-water facies of the Pierre Shale; 'brackish' corresponds to a nearshore, estuarine environment inhabited by lower salinity tolerant organisms (Iron Lightning Member of the Fox Hills Formation and the Hell Creek Formation); 'open ocean' corresponds to specimens collected from the Severn Formation and are considered to represent fully marine conditions; and 'freshwater' corresponds to unionid bivalves from the Hell Creek Formation. Specimens from the *B. compressus* zone are limited to the seaway itself, and were all collected from the Pierre Shale of South Dakota, representing a shallow environment several hundred kilometers from the shoreline.

Table 2 lists the Late Cretaceous samples by ammonite zone, paleoenvironment and species. Organisms are either nektonic (e.g., the ammonites, nautiloids and belemnite) or epifaunal (e.g., the bivalves and gastropods). All specimens have an aragonite shell, with the exception of the calcitic belemnite (sample K23). We also analyzed the calcite infill of sample WI-K1 to assess the diagenetic evolution of these samples.

2.3. Methods

Cretaceous and modern specimens were prepared for isotope measurement by flaking off portions of the shell using a scalpel, or were drilled using a rotary tool with a 1 mm carbide bur. For the modern nautilus, the region of growth for which we had temperature data was targeted, e.g., for nautilus captured in the wild and transferred to an aquarium, we sampled the most recent growth near the aperture of the shell, while for records of juvenile growth, the first seven septa were sampled. All shell fragments were cleaned with de-ionized water (DI) and a fine brush. Those with particles adhered to the shell were also sonicated in DI for 1–2 min and then rinsed. After air-drying the material, cleaned shell fragments were crushed to a fine powder using a small agate mortar and pestle, and weighed out into 5–8 mg samples.

Isotope measurements were made in the Laboratory for Geochemical Oceanography at Harvard University between September 2010 and November 2011. Using a common acid bath with 90 °C concentrated phosphoric acid (H_3PO_4), powdered carbonate samples were digested in acid for approximately 6 min and the product CO_2 was collected using liquid N_2, after passing through a −80 °C

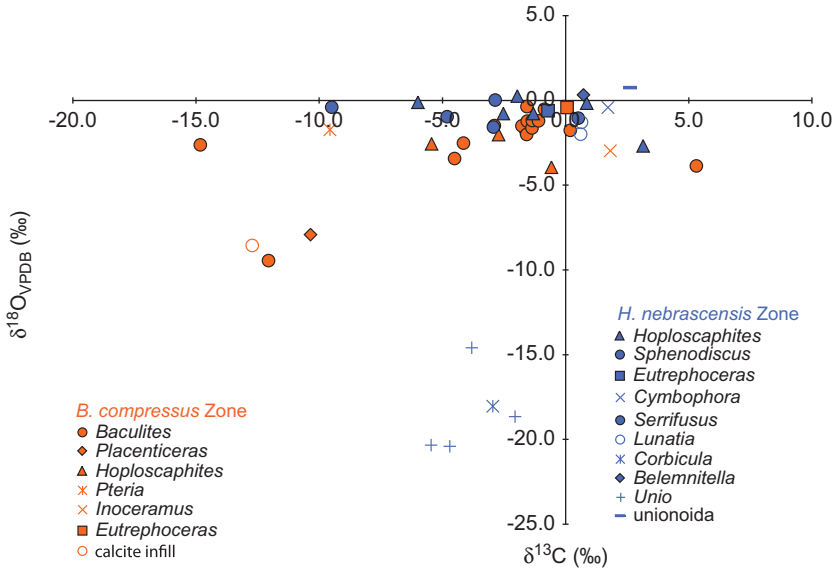

Fig. 1. Cross-plot of the bulk isotopic composition of Late Cretaceous macrofossils and the calcite infill of one specimen. Both $\delta^{13}C$ and $\delta^{18}O$ are reported relative to VPDB and the average 1σ standard error is 0.02‰ and 0.03‰, respectively. The samples are grouped by ammonite zone: *B. compressus* (orange) and *H. nebrascensis* (blue), and by genus (symbols in figure key). (For interpretation of the references to color in this figure legend, the reader is referred to the web version of this article.)

Table 2
Late Cretaceous sample identification and location, split by ammonite zone and paleoenvironment. The samples from the *B. compressus* Zone all represent the Interior Seaway, and no further paleoenvironmental details are available. The younger samples cover a range of paleoenvironments, and have been correlated to the *H. nebrascensis* ammonite zone. The first listing of the genus name is given in full, while further references to the genus are abbreviated. We also note that a recent change in nomenclature has resulted in the genus *Jelezkytes* being replaced by *Hoploscaphites*. The Museum IDs refer to: AMNH=American Museum of Natural History, YPM=Yale Peabody Museum, USNM=US National Museum.

Ammonite zone	Paleoenvironment	Sample	Location	Museum locality/specimen #	Species	Organism
B. compressus (~73.5 Ma)		WI-2	Pierre Shale, Meade County, SD	AMNH loc 3274	*Baculites compressus*	Ammonite
		WI-K1	Pierre Shale, Meade County, SD	AMNH loc 3274	*B. compressus*	Ammonite
		WI-K2 (*c*)	Pierre Shale, Meade County, SD	AMNH loc 3274	Calcite infill of WI-K1	
		WI-4	Pierre Shale, Meade County, SD	AMNH loc 3274	*B. compressus*	Ammonite
		WI-13B	Pierre Shale, Meade County, SD	AMNH loc 3274	*B. compressus*	Ammonite
		WI-17	Pierre Shale, Meade County, SD	AMNH loc 3274	*B. compressus*	Ammonite
		WI-40b	Pierre Shale, Meade County, SD	AMNH loc 3274	*B. compressus*	Ammonite
		WI-47	Pierre Shale, Meade County, SD	AMNH loc 3274	*B. compressus*	Ammonite
		WI-12	Pierre Shale, Meade County, SD	AMNH loc 3274	*Placenticeras meeki*	Ammonite
		WI-21	Pierre Shale, Meade County, SD	AMNH loc 3274	*Hoploscaphites brevis*	Ammonite
		WI-23A	Pierre Shale, Meade County, SD	AMNH loc 3274	*H. brevis*	Ammonite
		WI-32	Pierre Shale, Meade County, SD	AMNH loc 3274	*Pteria linguiformis*	Bivalve
		WI-37	Pierre Shale, Meade County, SD	AMNH loc 3274	Unknown	
		I-36	Pierre Shale, Meade County, SD	AMNH loc 3274	*H. nodosus*	Ammonite
		I-61	Pierre Shale, Meade County, SD	AMNH loc 3274	*Inoceramus*	Bivalve
		I-63	Pierre Shale, Meade County, SD	AMNH loc 3274	*Eutrephoceras dekayi*	Nautiloid
		I-62	Pierre Shale, Meade County, SD	AMNH loc 3274	*B. compressus*	Ammonite
		I-73	Pierre Shale, Pennington County, SD	AMNH loc 3383	*B. compressus*	Ammonite
		I-75	Pierre Shale, Pennington County, SD	AMNH loc 3383	*B. compressus*	Ammonite
		I-76	Pierre Shale, Pennington County, SD	AMNH loc 3383	*B. compressus*	Ammonite
		I-77	Pierre Shale, Pennington County, SD	AMNH loc 3383	*B. compressus*	Ammonite
		I-98	Pierre Shale, Meade County, SD	AMNH loc 3274	*B. compressus*	Ammonite
		I-101	Pierre Shale, Meade County, SD	AMNH loc 3274	*B. compressus*	Ammonite
		I-104	Pierre Shale, Meade County, SD	AMNH loc 3274	*B. compressus*	Ammonite
		I-106	Pierre Shale, Meade County, SD	AMNH loc 3274	*B. compressus*	Ammonite
		I-110	Pierre Shale, Meade County, SD	AMNH loc 3274	*B. compressus*	Ammonite
H. nebrascensis (~67 Ma)	Nearshore interior	K1	Timber Lake Mbr, Fox Hills	AMNH 45405	*H. nebrascensis*	Ammonite
	Nearshore interior	K5	Timber Lake Mbr, Fox Hills	AMNH 45463	*Sphenodiscus lobatus*	Ammonite
	Nearshore interior	K8	Timber Lake Mbr, Fox Hills	YPM 44980	*S. lobatus*	Ammonite
	Nearshore interior	K13	Timber Lake Mbr, Fox Hills	YPM 162433	*H. nebrascensis*	Ammonite
	Nearshore interior	K21	Timber Lake Mbr, Fox Hills	YPM 202291	*Cymbophora warreni*	Bivalve
	Nearshore interior	K10	Timber Lake Mbr, Fox Hills	YPM 162434	*Serrifusus dakotensis*	Gastropod
	Offshore interior	K23 (*c*)	Pierre Shale	USNM 486528	*Belemnitella* cf. *bulbosa*	Belemnite
	Offshore interior	K34	Pierre Shale	AMNH 47462	*S. lobatus*	Ammonite
	Offshore interior	K37	Pierre Shale	USNM 520477	*H. nebrascensis*	Ammonite
	Open ocean	K3	Severn Formation	AMNH 45406	*E. dekayi*	Nautiloid
	Open ocean	K4-A	Severn Formation	AMNH 45404	*S. lobatus*	Ammonite
	Open ocean	K35	Severn Formation	USNM 520476	*H. nebrascensis*	Ammonite
	Open ocean	K35-C	Severn Formation	USNM 520476-C	bivalve	Bivalve
	Brackish	K14	Iron Lightning Mbr, Fox Hills	YPM 162374	*H. nebrascensis*	Ammonite
	Brackish	K18	Iron Lightning Mbr, Fox Hills	YPM 162437	*H. nebrascensis*	Ammonite
	Brackish	K7	Timber Lake Mbr, Fox Hills	YPM 46036	*Tancredia americana*	Bivalve
	Brackish	K15	Iron Lightning Mbr, Fox Hills	YPM 162397,8	*Lunatia* sp.	Gastropod
	Brackish	K19	Hell Creek Formation	YPM 200285	*Lunatia* sp.	Gastropod
	Brackish	K9	Iron Lightning Mbr, Fox Hills	YPM 162385	*Corbicula* sp.	Bivalve
	Freshwater	K6	Hell Creek Formation	YPM 38033	*Unio* sp.	Bivalve
	Freshwater	K12	Hell Creek Formation	YPM 38034	*Unio* sp.	Bivalve
	Freshwater	K16	Hell Creek Formation	YPM 38029	*Unio* sp.	Bivalve
	Freshwater	K17	Hell Creek Formation	YPM 38005	*Unio* sp.	Bivalve
	Freshwater	K22	Hell Creek Formation	YPM 38044	Unionoida	Bivalve

ethyl-alcohol water trap. The evolved CO_2 was then purified using a static PoraPak Q trap on a glass vacuum line (Dennis and Schrag, 2010), and analyzed on a Thermo Finnigan MAT 253 for $\delta^{13}C$, $\delta^{18}O$ and Δ_{47}. We assessed the effectiveness of our purification procedure by monitoring Δ_{48}, an analogous parameter to Δ_{47}, during mass spectrometry (Eiler and Schauble, 2004; Huntington et al., 2009). The macrofossil and modern cephalopod Δ_{48} data aligned with our expectations based on measured heated and equilibrated gases, suggesting potential contaminant species such as chlorinated hydrocarbon were removed.

The MAT 253, which has been modified (as described in Dennis and Schrag, 2010), was operated in dual inlet mode and configured to measure masses 44–48 CO_2 through the following resistors: m/z 44 $= 3 \times 10^7\ \Omega$, m/z 45 $= 3 \times 10^9\ \Omega$, m/z 46 $= 1 \times 10^{10}\ \Omega$, m/z 47 $= 1 \times 10^{12}\ \Omega$, m/z 48 $= 1 \times 10^{12}\ \Omega$. Data was typically acquired by balancing at 2 V on mass 47, with masses 44, 45, 46 and 48 registering at approximately 1.2 V, 1.3 V, 1.6 V and 0.2 V, respectively. The equivalent currents are 40 nA, 0.04 nA, 0.02 nA, 2 pA and 0.2 pA, respectively. Each individual CO_2 sample was measured for one acquisition comprised of between 18 and 20 counts with four standard-sample-standard cycles per count. Ion integration time was 26 s per change over (1872–2080 s of total sample current integration time) and the bellows were pressure adjusted to balance at 2 V on mass 47 between each 4-cycle count. Individual samples were run for approximately 3 h on the MAT 253, and for a typical measurement protocol, approached the shot-noise limit to precision is 0.009‰ (Merritt and Hayes, 1994). Each carbonate sample was replicated, on average, three times requiring at least 15–20 mg of powdered carbonate per specimen. The data from each analysis was averaged and errors are reported based on replicate measurements.

Bulk measurements of $\delta^{18}O_c$ are corrected for acid fractionation at 90 °C (Swart et al., 1991), and along with $\delta^{13}C$, are reported relative to VPBD. Clumped isotope data (Δ_{47}) are projected into the absolute reference frame using heated and equilibrated CO_2 gas measurements (Supplementary Data Table 1). This reference frame empirically accounts for fragmentation and recombination reactions that occur in electron impact ionization sources, along with other mass spectrometric artifacts (Dennis et al., 2011).

We measured an in-house Carrara marble standard (CM2) 53 times during the measurement period, yielding an average $\Delta_{47}=0.388\pm0.005$‰ ($1\sigma$ standard error, SE), $\delta^{13}C=2.28\pm0.01$‰ and $\delta^{18}O_c=-1.78\pm0.01$‰. Three other carbonate standards were also measured sporadically. Given the accuracy of carbonate standard data during the measurement time period, no additional corrections have been made (Supplementary Data Table 2).

We convert Δ_{47} to temperature based on our analysis of modern cephalopods (Section 4.2). The calcification temperature can then be used to calculate the oxygen isotopic composition of the water ($\delta^{18}O_w$) in which the shell grew. For aragonite (all samples with the exception of WI-K2 and K23), the aragonite-water calibration of Grossman and Ku (1986) was used, where $\delta^{18}O_{aragonite}$ is vs. VPDB and $\delta^{18}O_w$ is vs. VSMOW:

$$T(^\circ C)=21.8-4.69\left(\delta^{18}O_{aragonite}-\delta^{18}O_w\right) \quad (1)$$

The VSMOW value for water in Eq. (1) is adjusted using −0.2 following the protocol of Grossman and Ku (1986). For calcite, the calibration of Kim and O'Neil (1997) was used, where temperature is expressed in Kelvin and α represents the fractionation factor between calcite and water:

$$1000\ln\alpha_{(calcite\text{-}water)}=18.03\left(10^3T^{-1}\right)-32.42 \quad (2)$$

Previously published Sr concentration data (Cochran et al., 2010; Cochran et al., 2003) and preservation indices for many of the Late Cretaceous samples are used to assess if the clumped isotope signatures are primary. The Preservation Index (PI) is a qualitative index which assesses the microstructure of nacreous shell material, as imaged by scanning electron microscopy (SEM) at AMNH (Cochran et al., 2010). Preservation is assigned an index from 5 (excellent preservation, showing distinct nacreous tablets) to 1 (poor preservation, in which the nacreous tablets have fused together). Even at poor preservation, the mineralogy remains aragonite (Cochran et al., 2010).

3. Results

3.1. Modern cephalopods

Table 1 shows the results for the modern cephalopods.[2] Included are the estimated growth temperatures, $\delta^{18}O_w$ values, and the measured bulk and clumped isotopic compositions. Values of $\delta^{13}C$ range from −3.13‰ to 2.07‰, and $\delta^{18}O_c$ ranges from −0.44‰ to 1.60‰. The Δ_{47} values range from 0.660‰ to 0.725‰ with an average measurement error of 0.011‰ (1σ SE). Also shown are the expected Δ_{47} values, as calculated from the known growth temperature and a synthetic calcite calibration of the clumped isotope thermometer (Ghosh et al., 2006) projected into the absolute reference frame (Dennis et al., 2011):

$$\Delta_{47}=\frac{(0.0636\pm0.0049)\times10^6}{T^2}-(0.0047\pm0.0520) \quad (3)$$

[2] Raw data for individual mass spectrometric analyses of both the modern cephalopods and Late Cretaceous macrofossils are complied in Supplementary Data Table 3.

The expected Δ_{47} values range from 0.720‰ to 0.761‰, and the difference between the expected and measured Δ_{47} values range from 0.022‰ to 0.099‰.

3.2. Cretaceous macrofossils

Table 3 shows the results for both the *B. compressus* ammonite zone and the *H. nebrascensis* ammonite zone. For the *B. compressus* zone $\delta^{13}C$ values range from −14.82‰ to 5.32‰ and $\delta^{18}O_c$ ranges from −9.46‰ to −0.37‰. The clumped isotope compositions range from 0.632‰ to 0.669‰ with an average measurement error of 0.008‰ (1σ SE). Taking the population average of the entire suite of *B. compressus* samples, the mean is 0.653 ± 0.002‰ (1σ SE). $\delta^{13}C$ values for the *H. nebrascensis* zone range from −9.48‰ to 3.15‰, and from −20.41‰ to 0.74‰ for $\delta^{18}O_c$. The clumped isotope compositions range from 0.646‰ to 0.729‰, with an average measurement error of 0.009‰ (1σ SE). Also reported in Table 3 are the corrected Δ_{47} values, clumped isotope temperature and calculated $\delta^{18}O_w$. These data are discussed in Sections 4.2 and 4.3.

For both zones, the majority of samples cluster between −5 and 1‰ in $\delta^{13}C$ and between −5 and 0‰ in $\delta^{18}O_c$ (Fig. 1). The exceptions are (i) the *Unio* and *Corbicula* bivalves which record much more depleted $\delta^{18}O_c$ ($\delta^{18}O_c=-14.6$ to −20.4‰), attributed to a freshwater setting (Cochran et al., 2003), and (ii) the depleted $\delta^{13}C$ values of two *Baculites* (WI-13B and WI-47), a *Placenticeras* (WI-12), a *Pteria* (bivalve; WI-32) and the calcite infill of a *Baculites* (WI-K2) from the *B. compressus* zone and a *Sphenodiscus* (K34) from the *H. nebrascensis* ammonite zone.

The specimens depleted in ^{13}C can be separated into distinct alteration groups. First, Cochran et al. (2010) documented decreases in $\delta^{18}O_c$, $\delta^{13}C$ and $^{87}Sr/^{86}Sr$ of *B. compressus* zone samples as preservation, as indexed by the PI value, declined and attributed the trends to diagenetic alteration, likely with meteoric water. The secondary calcite infill of the *Baculites* WI-K1 (WI-K2) aligns with this alteration regime. We suggest samples WI-47 and WI-12 also fall into this category of alteration, with WI-12 having additional support from its low visual preservation ($PI=1$). Second, those samples only depleted in $\delta^{13}C$ likely acquired their isotopic signature during early diagenesis in the presence of marine porewater depleted in ^{13}C due to the respiration of buried organic matter (Cochran et al., 2010). This type of alteration likely explains samples WI-13B, WI-32 and K34, which have light $\delta^{13}C$ signatures, but $\delta^{18}O_c$ values that are inline with other specimens and less visual evidence for alteration (the PI values of WI-32 and K34 are 4 and 3.5, respectively). A third possibility, is that isotopically depleted $\delta^{13}C$ and $\delta^{18}O$ signatures are the result of alteration associated with high temperatures during burial, but analyses of organic matter from well-preserved jaws of ammonites in the WIS (Gupta et al., 2008) suggest this is unlikely for specimens from South Dakota, such as those analyzed in the present study. This conclusion is further supported by the clumped isotope data presented here. Finally, recent sedimentalogical and isotopic work has documented the presence of methane seeps within the Pierre Shale of the WIS (Landman et al., 2012; Metz, 2010). Such seeps could explain carbonates isotopically depleted in ^{13}C, but they have not been found within the *H. nebrascensis* zone. Seeps are present within the *B. compressus* zone, but all specimens labeled WI- are from a common host rock concretion. As such, it seems unlikely that a relatively immobile bivalve (e.g., WI-32) could have been in contact with a seep while other specimens from the same concretion were not.

Regardless of the origin of depleted isotopic signatures, samples with depleted $\delta^{13}C$ values in the *B. compressus* zone record clumped isotope signatures that are towards the low end of the Δ_{47} range. Even so, removing samples WI-13B, WI-47, WI-12, WI-32 and WI-K2 from the population only shifts the mean Δ_{47} value by 0.003‰ (equivalent to <1 °C) to 0.656 ± 0.002‰.

Table 3
Results of bulk and clumped isotope analysis of Cretaceous macrofossils from the *B. compressus* and *H. nebrascensis* ammonite zones of the Western Interior Seaway. See Table 2 for additional details on the samples. All samples are from aragonite shells with the exception of WI-K2 (calcite infill) and K23 (calcitic belemnite). SEM PI refers to the preservation index, as defined in Cochran et al. (2010), and Sr concentrations are from Cochran et al. (2003) and Cochran et al. (2010). Bulk carbonate isotopic compositions ($\delta^{13}C$ and $\delta^{18}O_c$) are reported relative to VPDB. Δ_{47} errors are reported as the external standard error of the mean for samples replicated three or more times ($n \geq 3$), as the external standard deviation of the mean for samples replicated two times ($n=2$), or as the standard deviation of internal counting statistics for samples measured only one time ($n=1$). Corrected Δ_{47} accounts for the difference between the measured modern cephalopod Δ_{47} and the expected Δ_{47} (Table 1). Temperatures and $\delta^{18}O_w$ (reported relative to VSMOW) are calculated from the corrected Δ_{47} values using the synthetic calcite calibration of Ghosh et al. (2006) projected into the absolute reference frame (Eq. (3)). The statistics for populations of samples are reported as the mean and 1σ standard error. The error calculated for temperature and $\delta^{18}O_w$ does not account for uncertainty related to the offset between the measured Δ_{47} value of modern cephalopods and the expected Δ_{47} value, nor for other approaches to reconstructing temperature (Section 4.4).

Paleoenvironment	Sample	*n*	SEM PI	[Sr] (ppm)	$\delta^{13}C$ (‰)	$\delta^{18}O_c$ (‰)	Δ_{47} (‰)	Corrected Δ_{47} (‰)	Ghosh et al. (2006) calibration	
									T (°C)	$\delta^{18}O_w$ (‰)
B. compressus (~73.5 Ma)	WI-2	5	5		−1.59	−1.84	0.654 ± 0.010	0.713	24.7 ± 2.2	−1.0 ± 0.5
	WI-K1	3			−4.14	−2.52	0.643 ± 0.016	0.702	27.0 ± 3.6	−1.2 ± 0.8
	WI-K2 (c)	4			−12.72	−8.57	0.646 ± 0.007	0.705	26.2 ± 1.4	−6.0 ± 0.4
	WI-4	3	5		−1.76	−1.51	0.649 ± 0.002	0.708	25.6 ± 0.5	−0.5 ± 0.1
	WI-13B	1			−14.82	−2.64	0.644 ± 0.010	0.703	26.7 ± 2.1	−1.4 ± 0.4
	WI-17	3	4		0.20	−1.77	0.652 ± 0.010	0.711	25.0 ± 2.2	−0.9 ± 0.5
	WI-40b	1	4	1300	−1.36	−1.40	0.665 ± 0.011	0.724	22.2 ± 2.2	−1.1 ± 0.5
	WI-47	1			−12.05	−9.46	0.632 ± 0.009	0.691	29.3 ± 1.9	−7.7 ± 0.4
	WI-12	4	1	4530	−10.35	−7.93	0.651 ± 0.007	0.710	25.3 ± 1.5	−7.0 ± 0.3
	WI-21	3	5		−0.57	−3.94	0.644 ± 0.005	0.703	26.7 ± 1.0	−2.7 ± 0.2
	WI-23A	4	4		−5.44	−2.57	0.656 ± 0.008	0.715	24.2 ± 1.7	−1.8 ± 0.4
	WI-32	4	4		−9.56	−1.73	0.645 ± 0.007	0.704	26.4 ± 1.5	−0.5 ± 0.3
	WI-37	1			−2.42	−2.03	0.648 ± 0.009	0.707	25.9 ± 2.0	−1.0 ± 0.4
	I-36	1	3.5	3160	−2.72	−2.02	0.664 ± 0.011	0.723	22.5 ± 2.3	−1.7 ± 0.5
	I-61	3	4.5	1860	1.83	−2.97	0.669 ± 0.016	0.728	21.5 ± 3.2	−2.8 ± 0.7
	I-63	3	2	2850	0.07	−0.43	0.662 ± 0.002	0.721	23.0 ± 0.4	0.0 ± 0.1
	I-62	3	5		−1.54	−1.23	0.644 ± 0.004	0.703	26.6 ± 0.9	0.0 ± 0.2
	I-73	3	2.5		−1.56	−0.37	0.656 ± 0.011	0.715	24.2 ± 2.2	0.3 ± 0.5
	I-75	3	5		−0.86	−0.53	0.664 ± 0.004	0.723	22.5 ± 0.8	−0.2 ± 0.2
	I-76	3	4		−1.58	−2.02	0.662 ± 0.005	0.721	23.0 ± 1.1	−1.6 ± 0.3
	I-77	3	3.5		5.32	−3.87	0.664 ± 0.003	0.723	22.6 ± 0.6	−3.5 ± 0.1
	I-98	3	5		−1.35	−1.63	0.660 ± 0.009	0.719	23.4 ± 1.8	−1.1 ± 0.4
	I-101	3	1		−4.50	−3.44	0.663 ± 0.006	0.722	22.7 ± 1.2	−3.0 ± 0.3
	I-104	3	5		−1.34	−1.20	0.651 ± 0.013	0.710	25.3 ± 2.7	−0.3 ± 0.6
	I-106	3	5		−1.09	−1.21	0.663 ± 0.007	0.721	22.8 ± 1.5	−0.8 ± 0.3
	I-110	2	3.5		−2.89	−1.49	0.640 ± 0.007	0.699	27.6 ± 1.6	−0.1 ± 0.5
B. compressus (all)							0.653 ± 0.002	0.712	24.7 ± 0.4	−1.8 ± 0.4
***B. compressus* (excluding altered samples on the basis of $\delta^{13}C$)**							**0.656 ± 0.001**	**0.715**	**24.2 ± 0.4**	**−1.2 ± 0.2**
H. nebrascensis (~67 Ma)										
Nearshore interior	K1	3	4.5	3963	−1.31	−0.77	0.691 ± 0.009	0.750	17.2 ± 1.7	−1.6 ± 0.4
Nearshore interior	K5	3	4.5	4705	−4.80	−0.98	0.654 ± 0.003	0.713	24.5 ± 0.7	−0.2 ± 0.2
Nearshore interior	K8	3	3.5	4329	−2.92	−1.59	0.663 ± 0.001	0.722	22.8 ± 0.3	−1.2 ± 0.1
Nearshore interior	K13	1	5	4247	−2.52	−0.78	0.659 ± 0.008	0.718	23.5 ± 1.7	−0.2 ± 0.4
Nearshore interior	K21	4		1898	1.72	−0.43	0.683 ± 0.012	0.744	18.3 ± 2.4	−1.0 ± 0.5
Nearshore interior	K10	3	5	2297	0.52	−1.06	0.646 ± 0.006	0.705	26.2 ± 1.3	0.1 ± 0.3
H. nebrascensis—**Nearshore Interior**							**0.667 ± 0.007**	**0.725**	**22.1 ± 1.4**	**−0.7 ± 0.3**
Offshore interior	K23 (*c*)	3		1319	0.73	0.32	0.665 ± 0.009	0.723	22.4 ± 1.9	2.2 ± 0.4
Offshore interior	K34	6	3.5	3859	−9.48	−0.41	0.696 ± 0.020	0.755	16.5 ± 3.7	−1.3 ± 0.8
Offshore interior	K37	7	5	2520	−1.96	0.26	0.729 ± 0.013	0.788	10.3 ± 2.3	−2.0 ± 0.5
H. nebrascensis—**Offshore Interior**							**0.695 ± 0.018**	**0.756**	**16.4 ± 3.5**	**−0.4 ± 1.3**
Open Ocean	K3	3	5	3261	−0.71	−0.62	0.669 ± 0.008	0.728	21.6 ± 1.7	−0.5 ± 0.4
Open Ocean	K4-A	3	4.5	3018	−2.85	0.02	0.675 ± 0.003	0.734	20.3 ± 0.6	−0.1 ± 0.3
Open Ocean	K35	3	3	1890	−5.99	−0.11	0.670 ± 0.007	0.729	21.4 ± 1.4	0.0 ± 0.3
Open Ocean	K35-C	3			0.07	−0.39	0.678 ± 0.005	0.737	19.6 ± 1.0	−0.7 ± 0.2
H. nebrascensis—**Open Ocean**							**0.673 ± 0.002**	**0.732**	**20.7 ± 0.5**	**−0.3 ± 0.2**
Brackish	K14	4	4	2545	0.86	−0.17	0.674 ± 0.007	0.733	20.5 ± 1.4	−0.2 ± 0.4
Brackish	K18	2	3	2680	3.15	−2.68	0.667 ± 0.030	0.726	22.0 ± 6.0	−2.4 ± 0.9
Brackish	K7	3		2412	0.28	−2.12	0.666 ± 0.007	0.725	22.0 ± 1.5	−1.9 ± 0.4
Brackish	K15	3		1589	0.65	−1.31	0.668 ± 0.008	0.727	21.8 ± 1.6	−1.1 ± 0.4
Brackish	K19	3		2043	0.62	−2.01	0.670 ± 0.003	0.729	21.3 ± 0.7	−1.9 ± 0.2
Brackish	K9	3		667	−2.95	−18.05	0.691 ± 0.005	0.750	17.1 ± 1.0	−18.8 ± 0.2
H. nebrascensis—Brackish (all)							0.673 ± 0.004	0.732	20.8 ± 0.8	−4.4 ± 2.9
H. nebrascensis—**Brackish (excludes K9)**							**0.669 ± 0.001**	**0.728**	**21.5 ± 0.3**	**−1.5 ± 0.4**
Freshwater	K6	4		405	−5.45	−20.34	0.680 ± 0.008	0.739	19.3 ± 1.6	−20.7 ± 0.4
Freshwater	K12	4		504	−4.69	−20.41	0.687 ± 0.008	0.746	17.9 ± 1.5	−21.0 ± 0.3
Freshwater	K16	4		561	−2.04	−18.67	0.680 ± 0.011	0.739	19.4 ± 2.2	−19.0 ± 0.6
Freshwater	K17	3		355	−3.80	−14.60	0.681 ± 0.008	0.740	19.1 ± 1.6	−15.0 ± 0.4
Freshwater	K22	3			2.62	0.74	0.678 ± 0.010	0.736	19.8 ± 2.0	0.5 ± 0.5
H. nebrascensis—Freshwater (all)							0.681 ± 0.002	0.740	19.1 ± 0.3	−15.0 ± 4.0
H. nebrascensis—**Freshwater (excludes K22)**							**0.683 ± 0.002**	**0.741**	**18.9 ± 0.4**	**−18.9 ± 1.4**

4. Discussion

4.1. Burial alteration

Before reconstructing temperatures from the geologic record it is important to assess if the macrofossils are recording primary, environmental signatures. We discussed early diagenesis with respect to oxygen and carbon isotopes in Section 3.2. In addition, for carbonate clumped isotope thermometry the isotopic ordering of shell material must have remained intact since deposition if we are to determine past temperatures (Came et al., 2007; Finnegan et al., 2011; Huntington et al., 2011). Although macrofossils from the WIS are among some of the best preserved in the geologic record – many still retain the iridescent luster common to molluscs today – overburden and burial diagenesis could alter a macrofossil's state of isotopic ordering without significantly altering its bulk isotopic composition (Dennis and Schrag, 2010).

For those samples imaged by SEM, we plot the clumped isotope value recorded by a specimen against the PI (Fig. 2a). If burial diagenesis at elevated temperatures had occurred, the expected trend would be a positive correlation between SEM PI and Δ_{47}, i.e., a decrease in preservation associated with a decrease in Δ_{47}, or an increase in temperature. There is no trend in Δ_{47} with preservation suggesting alteration has not changed the clumped isotope signature of these samples. In general, the specimens from the *H. nebrascensis* zone (blue) cluster at higher Δ_{47} values, or lower temperatures. Specimens from the *B. compressus* zone (orange) span the entire range in preservation and there is no trend with clumped isotope composition. Although not all specimens were imaged, the Δ_{47} range recorded by the sub-set with PI values encompasses almost the entire range in Δ_{47}.

We also assess preservation by comparing Δ_{47} to Sr concentration. Cochran et al. (2010) showed that Sr/Ca ratios increase as preservation declines from excellent to poor, likely due to

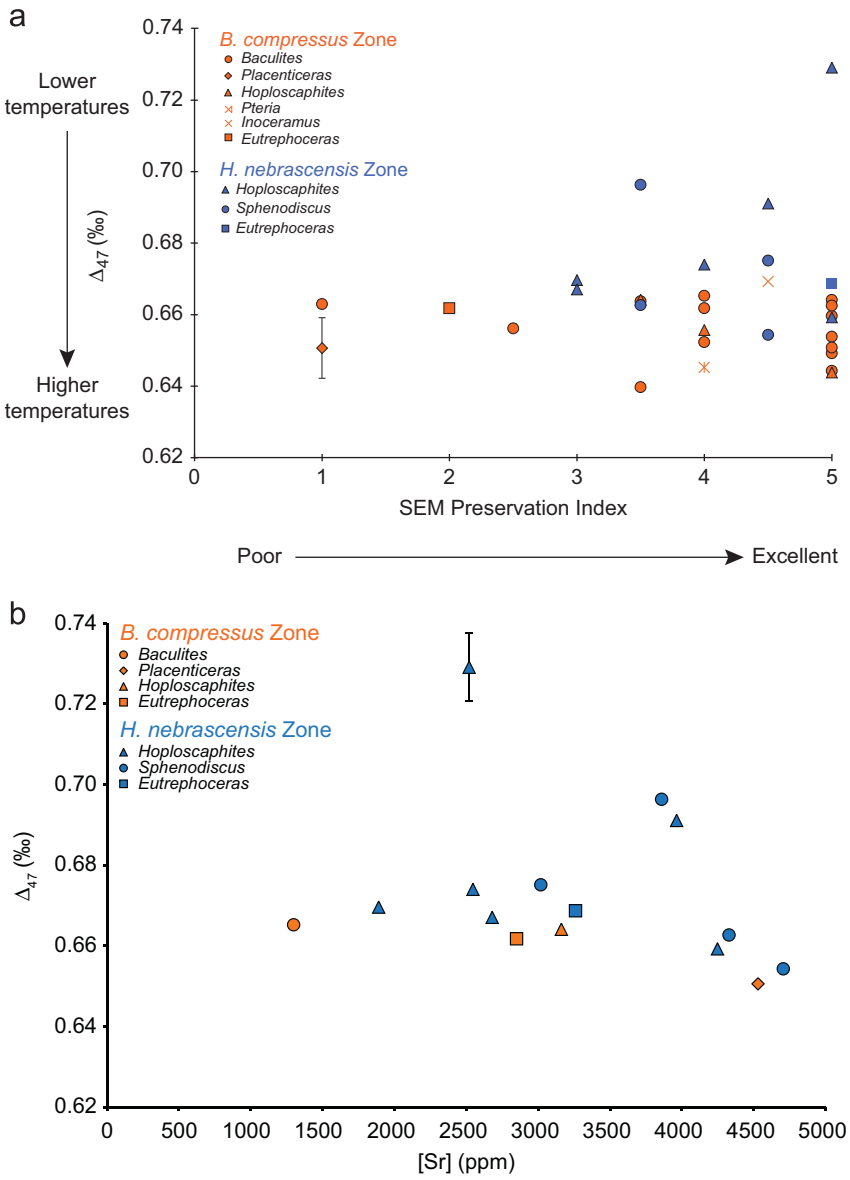

Fig. 2. (a) The qualitative Preservation Index (PI) plotted again the clumped isotopic composition of samples assessed by SEM. The samples are split by color: *B. compressus* Zone (orange) and *H. nebrascensis* Zone (blue). The average 1σ standard error in Δ_{47} is shown for one sample. (b) Sr concentration of ammonite samples from the *B. compressus* (orange) and *H. nebrascensis* (blue) Zones plotted against clumped isotopic composition (Δ_{47}). The Sr concentration data are from Cochran et al. (2003) and Cochran et al. (2010). Only ammonites are plotted to avoid taxonomic class effects of Sr incorporation, and variability in Sr across paleoenvironments. The average 1σ standard error in Δ_{47} is shown for one sample. (For interpretation of the references to color in this figure legend, the reader is referred to the web version of this article.)

strontianite precipitating between the nacreous tablets and fusing them together. In contrast, wholesale recrystallization to calcite (not observed in our specimens) results in loss of Sr from the mineral structure (Brand, 2004; Shields et al., 2003; Turekian and Armstrong, 1961). Given that our samples have not been recrystallized to calcite, if alteration had affected the Δ_{47} values, there should be an inverse relationship with Sr concentration. We find no such correlation between Sr and Δ_{47} in ammonites from the *B. compressus* and *H. nebrascensis* Zones (Fig. 2b), thereby providing additional evidence that the Late Cretaceous macrofossils are recording environmental conditions in their Δ_{47} signatures.

4.2. Disequilibrium precipitation in modern cephalopods

Modern nautilus and cuttlefish record clumped isotope signatures that are up to 0.1‰ lower than their expected Δ_{47} value, as calculated from the known growth temperature and Eq. (3) (Table 1). This suggests cephalopods are exhibiting a vital effect resulting in disequilibrium precipitation with respect to clumped isotopes. In contrast, most specimens precipitate shells within 1 °C of our expectation for bulk oxygen isotopes, equivalent to about ± 0.2‰ in $\delta^{18}O$. Whereas these small deviations from oxygen isotope equilibrium are reasonable given the errors associated with growth temperature and $\delta^{18}O_w$, imperfect knowledge of the growth environment cannot explain the apparent disequilibrium in clumped isotope measurements, which equates to an overestimate in temperature by up to 20 °C.

Clumped isotopic disequilibrium has also been recognized in other carbonates, most notably speleothems. These inorganic calcite cave deposits typically record apparent clumped isotope temperatures that are higher than the environmental growth temperature (Affek et al., 2008; Daëron et al., 2011; Meckler et al., 2009). Recent work has shown that the size of the clumped isotope kinetic isotope effect (KIE) can vary temporally, likely due to the degree of supersaturation and the strength of prior calcite precipitation (Kluge and Affek, 2012). Due to the large size of these clumped isotope KIEs, they can also be used as an indicator of disequilibrium in oxygen isotopes, even if other tests of disequilibrium precipitation are passed, e.g., the 'Hendy' test (Hendy, 1971; Kluge and Affek, 2012). Speleothems precipitate rapidly in response to CO_2 degassing, and it is hypothesized that incomplete oxygen isotope exchange in the remaining DIC pool is the cause of KIEs, resulting in clumped and oxygen isotope signatures that are disconnected from their local environment (Affek et al., 2008; Guo, 2008). While CO_2 degassing is not the relevant mechanism for cephalopods, biological control of CO_2 and DIC transport across cell membranes could yield similar effects (Thiagarajan et al., 2011).

Within the phylum Mollusca, bivalve shell formation is well understood (e.g., McConnaughey, 2003), and although the details are less constrained for the chambered nautilus, similarities exist (Crick and Mann, 2010). Both precipitate carbonate from the extrapallial fluid (EPF), which is isolated from the external environment and located between the mantle tissue and the existing shell (McConnaughey and Gillikin, 2008). The fluid is supplied with Ca^{2+} via ion pumping and exchange with H^+, resulting in an alkalinity gradient (McConnaughey, 2003; Shanahan et al., 2005). This gradient drives the diffusion of CO_2 into the EPF, where it is converted to HCO_3^- and CO_3^{2-} in the presence of carbonic anhydrase. The EPF can be greatly supersaturated with respect to $CaCO_3$ resulting in rapid calcification (McConnaughey and Gillikin, 2008). Possible isotopic evolutions of oxygen and clumped isotopes following diffusion, mixing or changes in pH were modeled by Thiagarajan et al. (2011), and although they found no evidence for disequilibrium precipitation of clumped isotopes in deep-sea corals, nor a process that altered Δ_{47} but not $\delta^{18}O_c$, biologically selective movement of ions could be the driving force behind clumped isotopic disequilibrium precipitation in modern cephalopods. Other calcifying organisms, e.g., foraminifera and corals, have a lower degree of control on biomineralization, perhaps explaining why foram tests appear to precipitate in clumped isotopic equilibrium (Thiagarajan et al., 2011; Tripati et al., 2010).

If the exchange of oxygen between water and DIC is what sets the isotopic composition of a precipitating carbonate, the expectation is that disequilibrium seen in clumped isotopes should also be apparent in oxygen isotopes. This is not the case for the modern cephalopod data presented here. As far as we are aware, this is the first example of disequilibrium clumped isotopes in the presence of equilibrium oxygen isotopes, although the reverse has been reported for deep-sea corals (Thiagarajan et al., 2011). Although we cannot currently confirm or refute any of the following explanations, we hypothesize that the apparent discrepancy between Δ_{47} and $\delta^{18}O_c$ seen in modern cephalopods could also be explained by: (i) inadequate knowledge of growth temperatures and/or $\delta^{18}O_w$, (ii) problems with the calibration of the carbonate clumped isotope thermometer, and/or (iii) methodological artifacts. In the case of (i), unidentified errors in the growth temperature and/or $\delta^{18}O_w$ could mean that the reported $\delta^{18}O_c$ values do not reflect equilibrium precipitation. For (ii), although many published biogenic and synthetic carbonates align with the original calibration of the clumped isotope thermometer, it is possible that this relationship does not represent isotopic equilibrium. Although unlikely, additional analyses of biogenic carbonates and synthetically precipitated aragonite and calcite could confirm or refute this. Likewise, testing how Δ_{47} responds to variable calcification rates, pH and saturation states could help further our understanding of isotopic equilibrium in the clumped isotope system. Finally for (iii), it is possible that the apparent disequilibrium in clumped isotopes for modern cephalopods is due to an analytical artifact, rather than being associated with a phenomenon in the carbonate system. For example, during acid digestion one third of the oxygen bound in carbonate is lost in the conversion to CO_2, thereby potentially breaking the ^{13}C–^{18}O bond we are interested in measuring. Earlier work (e.g., Ghosh et al., 2006; Passey et al., 2010) concluded this could be accounted for by using a simple correction, analogous to the acid fractionation factor utilized in traditional carbonate oxygen isotope measurements (Kim et al., 2007; Swart et al., 1991). It is possible that further, more detailed studies, may conclude that the fractionation factor varies with mineralogy and type of carbonate, possibly explaining the apparent disequilibrium clumped isotope signatures of cephalopods.

Fig. 3 plots the modern cephalopod data in the context of two synthetic calibrations of the clumped isotope thermometer (Dennis and Schrag, 2010; Ghosh et al., 2006), and a theoretical prediction (Guo et al., 2009). The limited temperature range of our data preclude us from developing a cephalopod-specific calibration, therefore we account for disequilibrium precipitation by calculating the offset between cephalopod Δ_{47} values and their expected Δ_{47} values (Ghosh et al., 2006; Eq. (3)). This calibration is selected because many other biogenic carbonates – corals, foraminifera, brachiopods, coccolithophorids, and some molluscs – have fallen on, or within error, of this calibration (for a review see Eiler, 2007, 2011). The average difference is 0.059 ± 0.019‰ (Table 1), and we apply this to the macrofossils prior to reconstructing temperature (compare the medium grey shaded region to the light grey shaded region in Fig. 3).

In so doing, we inherently assume that the cephalopods are recording environmental attributes but are offset from isotopic equilibrium due to vital effects (analogous to oxygen isotope

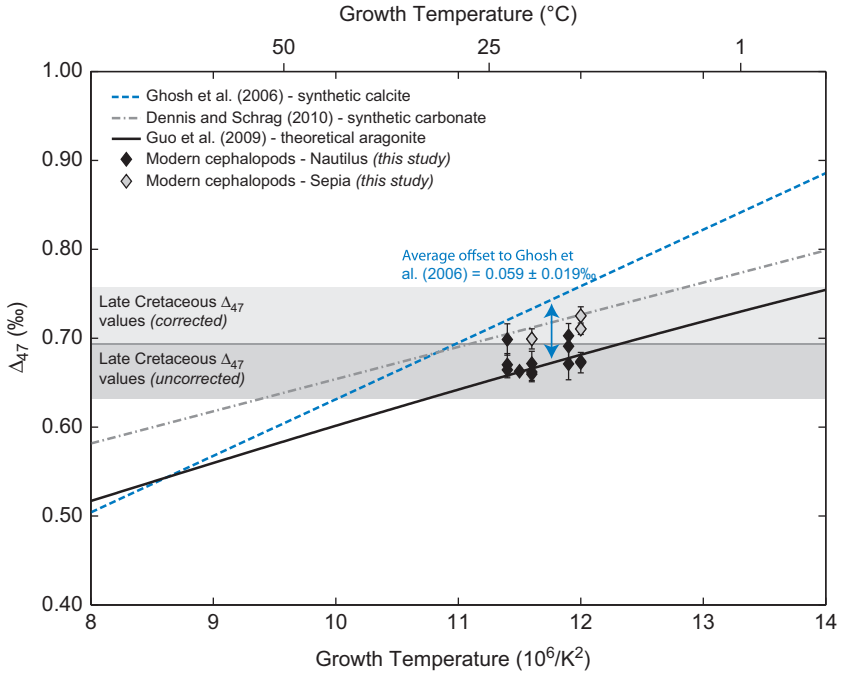

Fig. 3. Calibration of the carbonate clumped isotope thermometer, using known growth temperatures ($10^6/T^2$ in Kelvin) and measured Δ_{47} values. The top *x*-axis also shows the growth temperature in °C. Three different curves are plotted to help determine the most appropriate relationship for reconstructing paleotemperatures from Late Cretaceous macrofossils. The dashed blue line is the synthetic calcite calibration of Ghosh et al. (2006) and the dotted-dashed grey line is the synthetic carbonate calibration of Dennis and Schrag (2010). Both calibrations are projected into the absolute reference frame (Dennis et al., 2011). The black solid line is the theoretical prediction for aragonite (Guo et al., 2009). Also plotted are the modern cephalopod data from Table 1, along with their associated errors (when no error bars are present, the error is less than the size of the symbol). The blue arrow represents the average offset of the cephalopod data to the Ghosh et al. (2006) calibration. The shaded grey regions envelope the range of clumped isotope values measured in the Late Cretaceous macrofossils, excluding sample K37 (Table 3). The medium grey region covers the uncorrected values, the light grey region covers the corrected values, and the narrow dark grey band represents overlap between the populations. (For interpretation of the references to color in this figure legend, the reader is referred to the web version of this article.)

studies of some foraminfera, e.g., Duplessy et al., 1970; Graham et al., 1981; Katz et al., 2003; Shackleton et al., 1984), or an unknown analytical artifact. We also assume that this vital effect is constant with temperature and other environmental parameters, such as local salinity and pH, and that the biomineralization mechanisms in modern cephalopods are comparable to those in fossil molluscs. This is most applicable for the ammonites, which are morphologically similar to the modern nautilus. Likewise, consistent clumped isotope values for ammonites, bivalves and gastropods from the same biostratigraphic zone and location suggest that universal use of the modern cephalopod disequilibrium offset is valid. If different offsets, or calibrations, were used for bivalves, gastropods, and ammonites the resultant disparate temperatures and calculated $\delta^{18}O_w$ values from a common environment would be difficult to reconcile, although it is possible that the organisms lived at a different depths and calcified at different times of year.

4.3. *Reconstructing paleotemperatures and $\delta^{18}O_w$ in the Late Cretaceous*

By applying the modern cephaolopod correction to macrofossils, we reconstruct temperatures of between 16 and 22 °C for the Maastrichtian, and temperatures of about 24 °C for the Late Campanian (Table 3). For both the Late Campanian and the Maastrichtian, the calculated oxygen isotopic composition of the seaway and open-ocean approximately aligns with the expectation for an ice-free global ocean average of −1‰, relative to VSMOW (Shackleton and Kennett, 1975).

The average temperature recorded by *B. compressus* Zone macrofossils is 24.2 ± 0.4 °C, and the isotopic composition of the seaway is −1.2 ± 0.2‰ (all population average errors represent 1σ SE). For the *H. nebrascensis* Zone, the average temperature for the Nearshore Interior environment is 22.1 ± 1.4 °C with a calculated $\delta^{18}O_w$ of −0.7 ± 0.3‰. The Offshore Interior records cooler temperatures, at 16.4 ± 3.5 °C, with a corresponding $\delta^{18}O_w$ of −0.4 ± 1.3‰. For the open ocean setting, the population average temperature is 20.7 ± 0.5 °C, and the oxygen isotopic composition of seawater is calculated to be −0.3 ± 0.2‰. The brackish environment has an average temperature of 21.5 ± 0.3 °C, and a $\delta^{18}O_w$ of −1.5 ± 0.4‰. Lower temperatures are recorded for the freshwater environment, with a population average of 18.9 ± 0.4 °C, and a calculated freshwater $\delta^{18}O_w$ of −18.9 ± 1.4‰.

The Offshore Interior paleoenvironment records a much larger range in temperatures than the other settings. Sample K37 records a lower temperature than all other specimens, irrespective of paleoenvironment, and has poor reproducibility. Similarly, sample K34 reproduced poorly, and records a depleted $\delta^{13}C$ signature, suggestive of early diagenesis in the presence of isotopically depleted marine porewater. For both Offshore Interior ammonites, replicates were analyzed from the same bulk material therefore sampling different growth periods is unlikely to be the cause. We also have no reason to suspect analytical problems, as these specimens were measured during the same analytical sessions as other specimens. Even so, the presence of an identified contaminant or small-scale heterogeneity cannot be ruled out. The third specimen analyzed from the Offshore Interior was K23, a belemnite. This was the only calcite shell material we analyzed, and it yielded a higher temperature than the other two Offshore Interior ammonites. This could imply the disequilibrium offset is a function of mineralogy or biomineralization mechanism. But, given the temperature recorded by the belemnite aligns with the Nearshore Interior average, this also lends further support to previous work suggesting the temperature dependence of

clumping is not a function of carbonate mineralogy (Came et al., 2007; Eagle et al., 2010; Ghosh et al., 2006; Ghosh et al., 2007). Regardless, due to the large error in average Offshore Interior temperature relative to the other paleoenvironmental settings, we exclude it from our climatic interpretation.

4.3.1. Comparisons to other paleoclimatic evidence

Climate models of varying complexity have been used to probe our understanding of the Cretaceous greenhouse (Barron et al., 1995; Barron et al., 1993; Bush and Philander, 1997; Otto-Bliesner et al., 2002; Poulsen et al., 1999). Most are forced with elevated CO_2 concentrations and include a broad-scale representation of the paleogeography in the Cretaceous. Modeling studies of the Late Cretaceous find that, compared to the modern, the largest amount of surface heating is at the high latitudes, i.e., there is a decreased equator-to-pole temperature gradient, and that the globally-averaged atmospheric temperature is warmer than today (Bush and Philander, 1997; Otto-Bliesner et al., 2002). For the interior of North America, Bush and Philander (1997) predict an annual mean near-surface temperature of 15–20 °C, and a ± 15 °C seasonal cycle. Otto-Bliesner et al. (2002) predict a mean annual atmospheric temperature of between 20 and 25 °C, and an annual mean sea surface temperature (SST) of 18–24 °C. The temperatures estimated from these models align well with our reconstructions, suggesting the macrofossils are recording mean annual temperatures.

Results from this study can also be compared to temperatures estimated from leaf physiognomy and the distribution of warm-climate species. On the basis of fossil crocodilians in the Late Cretaceous, Markwick (1998) finds mean annual temperatures in excess of 14 °C were present through out the mid-latitudes, and also in coastal regions of the high latitudes. Using a climate-leaf analysis multivariate program and leaf margin analysis for fossil leaves from the interior of North America, Davies-Vollum (1997) suggests the 20 °C mean annual temperature isotherm was located at about 45°N during the earliest Palaeocene. During the Late Cretaceous, this isotherm was also predicted to be located between 40° and 50°N (Upchurch and Wolfe, 1993). Both the leaf physiognomy data and the extent of fossil crocodilians suggest mean annual temperatures of about 20 °C, as we find for the WIS, are reasonable.

4.3.2. Oxygen isotopic composition of the WIS

The Nearshore Interior and open ocean $\delta^{18}O_w$ values determined in this study are close to our expectation for an ice-free global ocean average. Therefore, either the precipitation to evaporation (P:E) ratio over mid-latitude North America was approximately one, or for the shallow seaway itself, enhanced evaporation was balanced by freshwater input from the Sevier and Laramide highlands to the west. The freshwater end-member is significantly more depleted at ~ −19‰. A comparison to the modern informs us that precipitation over the western US can be very depleted – less than −20‰ during the cold season months and at high altitude – and that the majority of this very depleted precipitation falls as snow (Dutton et al., 2005; Henderson and Shuman, 2009). Following the principles of Rayleigh distillation, precipitation becomes progressively more depleted with decreasing temperature, fraction of water vapor remaining in the cloud, and increasing altitude (Faure and Mensing, 2005; Rowley and Garzione, 2007). Simple calculations based on the fractionation between liquid and vapor, temperature change and degree of rain-out, confirm rainfall approaching -19‰ is plausible for an air mass temperature of 10 °C and 80% rain-out. Fig. 4 is a simple representation of this process as envisioned for the WIS, and illustrates that if the freshwater bivalves measured in this study are from large rivers re-charged by high-elevation runoff from the Sevier and Laramide highlands, they should record ^{18}O-depleted

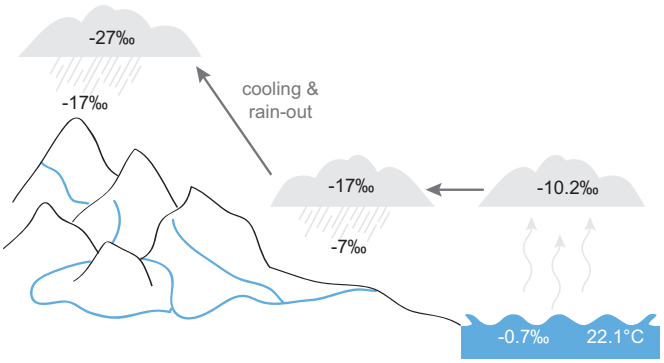

Fig. 4. An idealized schematic of oxygen isotopes in water vapor and precipitation to the west of the Interior Seaway.

waters. Temperatures for the freshwater environment are also approximately 3 °C cooler than the Interior Seaway, brackish and open ocean environments—a reasonable decrease if run-off is sourced from the highlands.

Depleted freshwater is also seen in other data sets from the region (e.g., Dettman and Lohmann, 2000; Fricke et al., 2010). These studies measured the carbonate isotopic composition of freshwater bivalves, and by making assumptions about the growth temperature of the bivalves, determined the average isotopic compositions of river water was −17‰. Both studies included samples from within tens of kilometers of the WIS shoreline, similar to the proximity of the Hell Creek Formation freshwater environment studied here (Johnson et al., 2002). Two mechanism for delivering such isotopically depleted waters have been proposed: (i) snowmelt (Dettman and Lohmann, 2000), and (ii) east to west monsoonal circulation driven by temperature contrasts between the warm seaway and the cold Sevier highlands (Fricke et al., 2010). Seasonal sampling of freshwater bivalves could differentiate between these scenarios. In the case of (i), we would expect the reconstructed $\delta^{18}O_w$ pattern to record the most depleted signatures during the spring when snowmelt is greatest. For (ii), we would expect the most depleted $\delta^{18}O_w$ values to coincide with the peak of convective precipitation during the summer months (Fricke et al., 2010). Fig. 4 also shows that a second population of freshwater bivalves should record an intermediate $\delta^{18}O_w$ signature closer to −7‰. This population would represent freshwater recharged locally on the low-lands (Fricke et al., 2010). Future work could target bivalves living in environments recharged by low-elevation rainfall, or land snails whose water is sourced directly from local precipitation, thereby refining our understanding of the precipitation regime west of the Late Cretaceous Interior Seaway.

For the paleoecologic groupings sampled within the *H. nebrascensis* Zone, it is possible to use our calculated $\delta^{18}O_w$ values to estimate the range of salinities in the WIS. Taking the freshwater input to be −18.9‰ and the open ocean to be −0.3‰ (with a salinity of 35), simple mixing predicts the brackish environment had a salinity of about 33. Although open ocean salinity may have differed from 35, our results suggest there was only a small gradient in salinity between the open ocean and brackish environments. This aligns with previous work based on $^{87}Sr/^{86}Sr$ (Cochran et al., 2003), which suggested that Sr isotope variations within the *H. nebrascensis* Zone (~67 Ma) of the WIS were not caused by salinity variations.

4.4. Sensitivity to vital effect corrections

If we apply the synthetic calibration of Dennis and Schrag (2010) directly to measured macrofossil Δ_{47} values reconstructed temperatures increase by, on average, 17 °C, and the oxygen isotopic composition of water is approximately 3–4‰ enriched

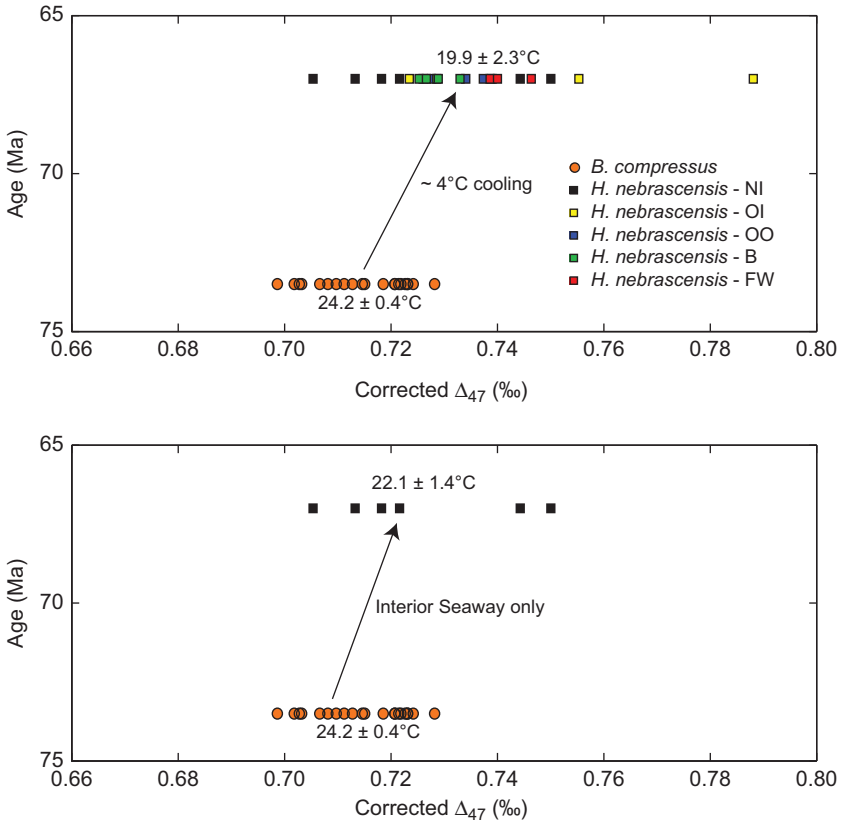

Fig. 5. Cooling over approximately 6 My between the *B. compressus* (~73.5 Ma) and *H. nebrascensis* (~67 Ma) ammonite zones. Macrofossils from the *B. compressus* Zone do not have further paleoenvironmental constraints above being associated with the WIS, therefore (a, top) compares all samples from the two ammonite zones, while (b, bottom) compares only those samples from the Interior Seaway. The Δ_{47} values are corrected using the difference between the measured Δ_{47} values of modern nautilus and the expected Δ_{47} given their growth environment (Table 1). The temperatures are calculated by applying the Ghosh et al. (2006) synthetic calcite calibration to the corrected Δ_{47} values.

compared to that calculated in the previous section[3]. Under this scenario, the average temperature of the *B. compressus* ammonite zone is 42.5 ± 0.8 °C, and the oxygen isotopic composition of the seaway is 2.7 ± 0.3‰, relative to VSMOW. The paleoenvironments of the *H. nebrascensis* ammonite zone record cooler temperatures than the *B. compressus* Zone—between 31 and 38 °C, excluding the Offshore Interior paleoenvironment. The seaway and open-ocean are enriched in ^{18}O, as compared to the ice-free global ocean average, and yield approximately the same $\delta^{18}O_w$ as the *B. compressus* Zone.

Similarly, if we use the synthetic calcite calibration of Ghosh et al. (2006) directly, without correcting for disequilibrium precipitation in modern cephalopods, seaway temperatures are also very warm, and the water is isotopically enriched compared to the expected global ocean average for the *B. compressus* Zone (~37 °C and $\delta^{18}O_w = 1.6$‰). For the *H. nebrascensis* ammonite zone temperatures decrease to between 29 and 35 °C.

We evaluate the likelihood of these significantly warmer climates, which are reconstructed when disequilibrium precipitation in modern cephalopods is ignored, in the context of other factors. First, although our assessment of burial alteration, based on SEM preservation and Sr concentrations, suggests the Δ_{47} values recorded by marine and freshwater macrofossils are primary, it is possible that micro-scale recrystallization or solid state diffusion has altered the clumped isotopic composition of these samples, even without altering the bulk oxygen isotopic composition (Eiler, 2011). Additional high resolution petrographic and trace metal analyses, for example electron backscatter diffraction and secondary ionization mass spectrometry, could provide additional evidence to confirm or refute the primary nature of the macrofossils studied here.

Second, the high temperatures inferred by direct use of either synthetic calibration could be artifacts of discontinuous growth through out the year. Many studies of modern molluscs (e.g., Schone et al., 2003; Ullmann et al., 2010; Weidman, Jones, 1994) show that during cold-season months the growth of skeletal carbonate slows or ceases entirely. Likewise, some molluscs slow their growth rate at very high temperatures (Schone et al., 2003). If carbonate precipitation is skewed to the warm season months, reconstructed temperatures between 25 and 35 °C would align with modeled peak summertime temperatures (Bush and Philander, 1997). But, temperatures higher than 35 °C, even for the summertime peak, seem unrealistically high. Tropical SSTs, from climate models and paleotemperature reconstructions from DSDP/ODP cores, predict temperatures to be no higher than 32 °C in the Late Cretaceous (Barrera and Savin, 1999; Bush and Philander, 1997; Otto-Bliesner et al., 2002; Poulsen et al., 1999). Similarly, paleontological comparisons of ammonites to their close living relative, the modern Nautilus, suggest temperatures in excess of 30 °C are unlikely. Indeed, Fatherree et al. (1998) performed a detailed sclerochronologic analysis of a baculite from the *B. compressus* Zone and found that temperatures (based on $\delta^{18}O_c$) ranged from 19.7 to 29.7 °C. Additional high-resolution sampling of Late Cretaceous macrofossils would help test whether a temporal record of

[3] Alternative calculations of temperature and $\delta^{18}O_w$ are included in Supplementary Data Table 3.

seasonality in both $\delta^{18}O_c$ and Δ_{47} is present, assuming that Late Cretaceous ammonites and bivalves biomineralize throughout the year and in isotopic equilibrium with water.

Third, we can use the calculated oxygen isotopic composition of water to assess if direct use of the synthetic carbonate calibrations is valid. Using these calibrations, $\delta^{18}O_w$ values range from approximately $-17‰$ for the freshwater environment to about $+2‰$ for the open ocean and Nearshore Interior seaway. The $+3‰$ enrichment of the open ocean and the Interior Seaway, as compared to the ice-free global ocean average, requires a P:E ratio of significantly less than one. In the surface ocean today, there are a few regions enriched by more than $+1.5‰$, as compared to the global ocean average (LeGrande and Schmidt, 2006). The exceptions are the eastern edge of the Mediterranean Sea and the northwest corner of the Red Sea, both of which have restricted circulation and are not appropriate modern analogs to the Late Cretaceous WIS based on their depth and meridional position. A more suitable analog would be the subtropical North Atlantic, which is enriched in ^{18}O by about 1.5‰—still only half of what is required in the Late Cretaceous if the synthetic calibrations are used directly.

In summary, the Late Cretaceous climate reconstructed by applying our Δ_{47} data directly to published synthetic carbonate calibrations is too warm. Similarly, the isotopic enrichment calculated for mid-latitude seas using these reconstructed temperatures is greater than that seen today. This provides further support for a cephalopod clumped isotope vital effect and validates our application of the modern cephalopod offset to fossil specimens. We conclude that without this correction the reconstructed temperatures and $\delta^{18}O_w$ values are incompatible with other climatic indicators.

4.5. Evidence for Late Cretaceous cooling

Irrespective of the calibration used, reconstructed temperatures from the Late Campanian and the Maastrichtian are consistent with a cooling trend over 6 My. Based on a comparison of the *B. compressus* Interior Seaway macrofossils to the entire population of macrofossils from the *H. nebrascensis* ammonite zone, temperatures decrease by about 4 °C from 24.2 ± 0.4 °C to 19.9 ± 2.3 °C (Fig. 5a). Temperature change in the seaway itself is not statistically significant (Fig. 5b), but it is consistent with cooling. These results align well with other reconstructions of temperature change over the Late Campanian and Maastrichtian, providing further evidence that the WIS macrofossils are recording primary clumped isotope compositions.

Reconstructions of deep-sea temperatures based on the $\delta^{18}O$ of benthic and planktonic foraminifera also record a cooling trend over the 10 My leading up to the Cretaceous-Tertiary boundary (Barrera and Savin, 1999). Most ocean basins record a benthic $\delta^{18}O$ increase of about 1‰ (Cramer et al., 2009; Friedrich et al., 2009; Li and Keller, 1999), which translates to a cooling of between 4 and 5 °C, if there is no contribution from a change in continental ice. The growth of small ephemeral ice sheets is unlikely because the North Atlantic basin shows little change in benthic $\delta^{18}O$ across the same time period (Huber et al., 2002; MacLeod et al., 2005). If changes in continental ice volume were responsible for the increase in $\delta^{18}O$, it should be recorded as an ocean-wide increase in $\delta^{18}O$. Our results, which record cooling rather than a shift in $\delta^{18}O_w$, also support the conclusion that the increase in benthic $\delta^{18}O$ is driven by temperature change, and not ice volume effects.

5. Conclusions

We have reconstructed the temperature and oxygen isotopic composition of the Late Creataceous WIS using a vital effect correction based on measuring modern cephalopods, close living relatives of the Cretaceous ammonites. Temperatures recorded in the WIS and surrounding environments are between 16 and 22 °C for the Maastrichtian, and are about 24 °C for the Late Campanian. These temperatures align with climate models (Bush and Philander, 1997; Otto-Bliesner et al., 2002) and paleoclimate reconstructions based on leaf physiognomy and the distribution of warm-climate flora and fauna (Davies-Vollum, 1997; Markwick, 1998). The seaway and open ocean environments have an oxygen isotopic composition approximately equal to the ice-free global ocean average of $-1‰$. The isotopically depleted freshwater end-member ($\delta^{18}O_w \sim -19‰$) is reasonable given run-off from the highlands to the west of the basin.

Unless micro-scale recrystallization has altered the clumped isotopic composition of the macrofossils, reconstructed temperatures using synthetic carbonate calibrations of the clumped isotope thermometer directly, i.e., without applying a correction based on our analysis of modern cephalopods, are unrealistically high. Likewise, the calculated $\delta^{18}O_w$ values are significantly more enriched than today's most isolated and saline oceanic basins (LeGrande and Schmidt, 2006).

The results for the WIS align with open-ocean benthic $\delta^{18}O$ reconstructions (Barrera and Savin, 1999; Cramer et al., 2009; Friedrich et al., 2009; Li and Keller, 1999) providing further evidence for global cooling during the latest Cretaceous.

Future work should focus on understanding why modern cephalopods record clumped isotope compositions that are in disequilibrium with the surrounding environment, and how biomineralization differences lead to an offset between the modern nautilus, cuttlefish and bivalves, and other skeletal carbonates, e.g., foraminifera and corals. In addition, expanding this study by reconstructing seasonal cycles in temperature and $\delta^{18}O$ for Late Cretaceous ammonites and bivalves will provide further constraints on the climate system.

Acknowledgments

Modern cephalopods and Late Cretaceous macrofossils analyzed in this study were graciously provided by the American Museum of Natural History (Loan numbers 503, 509 and 512), the Yale Peabody Museum (Loan number 908), Kazushige Tanabe at the University of Tokyo, and Felix Mark and Anne Thonig from the Alfred Wegner Institute. An earlier version of this manuscript was a component of K. Dennis' Ph.D. thesis and benefited from insightful comments from her committee members, David Johnston, Eli Tziperman and Peter Huybers. We thank Greg Henkes and Ben Passey for sharing unpublished modern mollusc data that aided in our discussion of disequilibrium precipitation, and Kathleen Sarg for the SEM work. This work was supported by Henry and Wendy Breck (to K.J.D. and D.P.S.), the Norman D. Newell Fund of the AMNH (to N.H.L. and J.K.C.), and NSF EAR Grant nos. 0308926 (to N.H.L.) and 0309343 (to J.K.C.). This is Contribution no. 1414 from the School of Marine and Atmospheric Sciences.

Appendix A. Supporting information

Supplementary data associated with this article can be found in the online version at http://dx.doi.org/10.1016/j.epsl.2012.11.036.

References

Affek, H.P., Bar-Matthews, M., Ayalon, A., Matthews, A., Eiler, J.M., 2008. Glacial/interglacial temperature variations in Soreq cave speleothems as recorded by 'clumped isotope' thermometry. Geochim. Cosmochim. Acta 72, 5351–5360.

Arthur, M.A., Dean, W.E., Schlanger, S.O., 1985. Variations in the global carbon cycle during the Cretaceous related to climate, volcanism, and changes in atmospheric CO_2. In: Sundquist, E.T., Broecker, W.S. (Eds.), The carbon cycle and atmospheric CO_2: Natural variations Archean to present. American Geophysical Union Geophysical Monograph, pp. 504–529.

Barrera, E., Savin, S.M., 1999. Evolution of late Campanian–Maastrichtian marine climates and oceans. Geological Society of America Special Paper 332, 245–282.

Barron, E.J., 1983. A warm, equable Cretaceous—the nature of the problem. Earth-Sci. Rev. 19, 305–338.

Barron, E.J., 1985. Numerical climate modeling, a frontier in petroleum source rock prediction: results based on Cretaceous similuations. AAPG Bull.-Am. Assn. Petrol. Geol. 69, 448–459.

Barron, E.J., Fawcett, P.J., Peterson, W.H., Pollard, D., Thompson, S.L., 1995. A "simulation" of mid-Cretaceous climate. Paleoceanography 10, 953–962.

Barron, E.J., Fawcett, P.J., Pollard, D., Thompson, S., 1993. Model simulation of cretaceous climates: the role of geography and carbon dioxide. Philos. Trans. R. Soc. London B 341, 307–315.

Bemis, B.E., Spero, H.J., Bijma, J., Lea, D.W., 1998. Reevaluation of the oxygen isotopic composition of planktonic foraminifera: experimental results and revised paleotemperature equations. Paleoceanography 13, 150–160.

Berner, R.A., Lasaga, A.C., Garrels, R.M., 1983. The carbonate-silicate geochemical cycle and its effect on atmospheric carbon-dioxide over the past 100 million years. Am. J. Sci. 283, 641–683.

Brand, U., 2004. Carbon, oxygen and strontium isotopes in Paleozoic carbonate components: an evaluation of original seawater-chemistry proxies. Chem. Geol. 204, 23–44.

Bush, A.B.G., Philander, S.G.H., 1997. The late Cretaceous: simulation with a coupled atmosphere-ocean general circulation model. Paleoceanography 12, 495–516.

Came, R.E., Eiler, J.M., Veizer, J., Azmy, K., Brand, U., Weidman, C.R., 2007. Coupling of surface temperatures and atmospheric CO_2 concentrations during the Palaeozoic era. Nature 449, 198–201.

Clarke, L.J., Jenkyns, H.C., 1999. New oxygen isotope evidence for long-term Cretaceous climatic change in the Southern Hemisphere. Geology 27, 699–702.

Clarkson, E.N.K., 1998. Invertebrate Palaeontology and Evolution. Blackwell Science.

Cobban, W.A., Walaszczyk, I., Obradovich, J.D., McKinney, K.C., 2006. A USGS zonal table for the upper Cretaceous middle Cenomanian–Maastrichtian of the Western Interior of the United States based on ammonites, inoceramids, and radiometric ages. US Geological Survey Open-File Report 2006-1250, 45 p.

Cochran, J.K., Kallenberg, K., Landman, N.H., Harries, P.J., Weinreb, D., Turekian, K.K., Beck, A.J., Cobban, W.A., 2010. Effect of diagenesis on the Sr, O and C isotope composition of Late Cretaceous mollusks from the Western Interior Seaway of North America. Am. J. Sci. 310, 69–88.

Cochran, J.K., Landman, N.H., Turekian, K.K., Michard, A., Schrag, D.P., 2003. Paleoceanography of the Late Cretaceous (Maastrichtian) Western Interior Seaway of North America: evidence from Sr and O isotopes. Palaeogeogr. Palaeoclimatol. Palaeoecol. 191, 45–64.

Coulson, A.B., Kohn, M.J., Barrick, R.E., 2011. Isotopic evaluation of ocean circulation in the Late Cretaceous North American seaway. Nat. Geosci. 4, 852–855.

Cramer, B.S., Miller, K.G., Barrett, P.J., Wright, J.D., 2011. Late Cretaceous–Neogene trends in deep ocean temperature and continental ice volume: reconciling records of benthic foraminiferal geochemistry ($\delta^{18}O$ and Mg/Ca) with sea level history. J. Geophys. Res. 16, 12023.

Cramer, B.S., Toggweiler, J.R., Wright, J.D., Katz, M.E., Miller, K.G., 2009. Ocean overturning since the Late Cretaceous: inferences from a new benthic foraminiferal isotope compilation. Paleoceanography 24, PA4216.

Crick, R.E., Mann, K.O., 2010. Biomineralization and systematic implications. In: Saunders, W.B., Landman, N.H. (Eds.), Nautilus—The Biology and Paleobiology of a Living Fossil. Springer, New York, pp. 115–136.

Daëron, M., Guo, W., Eiler, J., Genty, D., Blamart, D., Boch, R., Drysdale, R., Maire, R., Wainer, K., Zanchetta, G., 2011. $^{13}C^{18}O$ clumping in speleothems: observations from natural caves and precipitation experiments. Geochim. Cosmochim. Acta 75, 3303–3317.

Davies-Vollum, K.S., 1997. Early Palaeocene palaeoclimatic inferences from fossil floras of the western interior, USA. Palaeogeogr. Palaeoclimatol. Palaeoecol. 136, 145–164.

Dennis, K.J., Affek, H.P., Passey, B.H., Schrag, D.P., Eiler, J.M., 2011. Defining an absolute reference frame for 'clumped' isotope studies of CO_2. Geochim. Cosmochim. Acta 75, 7117–7131.

Dennis, K.J., Schrag, D.P., 2010. Clumped isotope thermometry of carbonatites as an indicator of diagenetic alteration. Geochim. Cosmochim. Acta 74, 4110–4122.

Dettman, D.L., Lohmann, K.C., 2000. Oxygen isotope evidence for high-altitude snow in the Laramide Rocky Mountains of North America during the Late Cretaceous and Paleogene. Geology 28, 243–246.

Douglas, R.G., Savin, S.M., 1975. Oxygen and carbon isotope analyses of Tertiary and Cretaceous macrofossils from the Shatsky Rise and other sites in the North Pacific Ocean. Initial Rep. Deep Sea Drilling Proj. 32, 509–520.

Duplessy, J.C., Lalou, C., Vinot, A.C., 1970. Differential isotopic fractionation in benthic foraminifera and paleotemperatures reasssessed. Science 168, 250–251.

Dutton, A., Wilkinson, B.H., Welker, J.M., Bowen, G.J., Lohmann, K.C., 2005. Spatial distribution and seasonal variation in $^{18}O/^{16}O$ of modern precipitation and river water across the conterminous USA. Hydrol. Process. 19, 4121–4146.

Eagle, R.A., Schauble, E.A., Tripati, A.K., Tutken, T., Hulbert, R.C., Eiler, J.M., 2010. Body temperatures of modern and extinct vertebrates from ^{13}C–^{18}O bond abundances in bioapatite. Proc. Natl. Acad. Sci. USA 107, 10377–10382.

Eiler, J.M., 2007. "Clumped-isotope" geochemistry—The study of naturally-occurring, multiply-substituted isotopologues. Earth Planet. Sci. Lett. 262, 309–327.

Eiler, J.M., 2011. Paleoclimate reconstruction using carbonate clumped isotope thermometry. Quat. Sci. Rev. 30, 3575–3588.

Eiler, J.M., Schauble, E., 2004. $^{18}O^{13}C^{16}O$ in Earth's atmosphere. Geochim. Cosmochim. Acta 68, 4767–4777.

Epstein, S., Buchsbaum, R., Lowenstam, H., Urey, H.C., 1951. Carbonate–water isotopic temperature scale. Geol. Soc. Am. Bull. 62, 417–426.

Erez, J., 1978. Vital effect on stable-isotope composition seen in foraminifera and coral skeletons. Nature 273, 199–202.

Fatherree, J.W., Harries, P.J., Quinn, T.M., 1998. Oxygen and carbon isotopic "dissection" of Baculites compressus (Mollusca: Cephalopoda) from the pierre shale (Upper Campanian) of South Dakota: implications for paleoenvironmental reconstructions. Palaios 13, 376–385.

Faure, G., Mensing, T.M., 2005. Isotopes: Principles and Applications, 3rd ed. John Wiley and Sons, Inc.

Finnegan, S., Bergmann, K., Eiler, J.M., Jones, D.S., Fike, D.A., Eisenman, I., Hughes, N.C., Tripati, A.K., Fischer, W.W., 2011. The magnitude and duration of Late Ordovician-Early Silurian Glaciation. Science 331, 903–906.

Fricke, H.C., Foreman, B.Z., Sewall, J.O., 2010. Integrated climate model-oxygen isotope evidence for a North American monsoon during the Late Cretaceous. Earth Planet. Sci. Lett. 289, 11–21.

Friedrich, O., Herrle, J.O., Wilson, P.A., Cooper, M.J., Erbacher, J., Hemleben, C., 2009. Early Maastrichtian carbon cycle perturbation and cooling event: implications from the South Atlantic Ocean. Paleoceanography, 24.

Ghosh, P., Adkins, J., Affek, H., Balta, B., Guo, W.F., Schauble, E.A., Schrag, D., Eiler, J.M., 2006. $^{13}C^{18}O$ bonds in carbonate minerals: a new kind of paleothermometer. Geochim. Cosmochim. Acta 70, 1439–1456.

Ghosh, P., Eiler, J., Campana, S.E., Feeney, R.F., 2007. Calibration of the carbonate 'clumped isotope' paleothermometer for otoliths. Geochim. Cosmochim. Acta 71, 2736–2744.

Graham, D.W., Corliss, B.H., Bender, M.L., Keigwin, L.D., 1981. Carbon and oxygen isotopic disequilibrium of recent deep-sea benthic foraminifera. Mar. Micropaleontol. 6, 483–497.

Grossman, E.L., Ku, T.L., 1986. Oxygen and carbon isotope fractionation in biogenic aragonite: temperature effects. Chem. Geol. 59, 59–74.

Guo, W., 2008. Carbonate clumped isotope thermometry: application to carbonaceous chondrites and effects of kinetic isotope fractionation. California Institute of Technology.

Guo, W.F., Mosenfelder, J.L., Goddard, W.A., Eiler, J.M., 2009. Isotopic fractionations associated with phosphoric acid digestion of carbonate minerals: insights from first-principles theoretical modeling and clumped isotope measurements. Geochim. Cosmochim. Acta 73, 7203–7225.

Gupta, N.S., Briggs, D.E.G., Landman, N.H., Tanabe, K., Summons, R.E., 2008. Molecular structure of organic components in cephalopods: evidence for oxidative cross linking in fossil marine invertebrates. Org. Geochem. 39, 1405–1414.

Habicht, J.K.A., 1979. Paleoclimate, paleomagnetism, and continental drift. Am. Assoc. Petrol. Geol. Geol. Stud. 9, 110.

Hancock, J.M., Kauffman, E.G., 1979. The great transgressions of the Late Cretaceous. J. Geol. Soc. London 136, 175–186.

Hay, W.W., 2008. Evolving ideas about the Cretaceous climate and ocean circulation. Cretaceous Res. 29, 725–753.

He, S., Kyser, T.K., Caldwell, W.G.E., 2005. Paleoenvironment of the Western Interior Seaway inferred from $\delta^{18}O$ and $\delta^{13}C$ values of molluscs from the Cretaceous Bearpaw marine cyclothem. Palaeogeogr. Palaeoclimatol. Palaeoecol. 217, 67–85.

Henderson, A.K., Shuman, B.N., 2009. Hydrogen and oxygen isotopic compositions of lake water in the western United States. Geol. Soc. Am. Bull. 121, 1179–1189.

Hendy, C.H., 1971. The isotopic geochemistry of speleothems—I. The calculation of the effects of different modes of formation on the isotopic composition of speleothems and their applicability as palaeoclimatic indicators. Geochim. Cosmochim. Acta 35, 801–824.

Herman, A.B., Spicer, R.A., 1997. New quantitative palaeoclimate data for the Late Cretaceous Arctic: evidence for a warm polar ocean. Palaeogeogr. Palaeoclimatol. Palaeoecol. 128, 227–251.

Huber, B.T., Hodell, D.A., Hamilton, C.P., 1995. Middle–Late Cretaceous climate of the southern high latitudes: stable isotopic evidence for minimal equator-to-pole thermal gradients. Geol. Soc. Am. Bull. 107, 1164–1191.

Huber, B.T., Norris, R.D., MacLeod, K.G., 2002. Deep-sea paleotemperature record of extreme warmth during the Cretaceous. Geology 30, 123–126.

Huntington, K.W., Budd, D.A., Wernicke, B.P., Eiler, J.M., 2011. Use of clumped-isotope thermometry to constrain the crystallization temperature of diagenetic calcite. J. Sediment. Res. 81, 656–669.

Huntington, K.W., Eiler, J.M., Affek, H.P., Guo, W., Bonifacie, M., Yeung, L.Y., Thiagarajan, N., Passey, B., Tripati, A., Daëron, M., Came, R., 2009. Methods and limitations of 'clumped' CO_2 isotope (Δ_{47}) analysis by gas-source isotope ratio mass spectrometry. J. Mass Spectrom. 4,, 318–329.

Hut, G., 1987. Consultants group meeting on stable istope reference samples for geochemical and hydrological investigations. Report to the Director General. International Atomic Energy Agency, Vienna, pp. 42.

Johnson, K.R., Nichols, D.J., Hartman, J.H., 2002. Hell Creek Formation: a 2001 synthesis. In: Hartman, J.H., Johnson, K.R., Nichols, D.J. (Eds.), The Hell Creek

Formation and the Cretaceous-Tertiary boundary in the northern Great Plains: An integrated continental record of the end of the Cretaceous. Geological Society of America, pp. 503–510.
Katz, M.E., Katz, D.R., Wright, J.D., Miller, K.G., Pak, D.K., Shackleton, N.J., Thomas, E., 2003. Early Cenozoic benthic foraminiferal isotopes: species reliability and interspecies correction factors. Paleoceanography 18, 1024.
Kauffman, E.G., 1984. Paleobiogeography and evolutionary response dynamic in the Cretaceous Western Interior Seaway of North America. In: Westermann, G.E.G. (Ed.), Jurassic–Cretaceous Biochronology and Paleogeography of North America. Geological Association of Canada, pp. 273–306.
Kennedy, W.J., Landman, N.H., Christensen, W.K., Cobban, W.A., Hancock, J.M., 1998. Marine connections in North America during the late Maastrichtian: palaeogeographic and palaeobiogeographic significance of Jeletzkytes nebrascensis Zone cephalopod fauna from the Elk Butte Member of the Pierre Shale, SE South Dakota and NE Nebraska. Cretaceous Res. 19, 745–775.
Kim, S.T., Mucci, A., Taylor, B.E., 2007. Phosphoric acid fractionation factors for calcite and aragonite between 25 and 75 °C: revisited. Chem. Geol. 246, 135–146.
Kim, S.T., O'Neil, J.R., 1997. Equilibrium and nonequilibrium oxygen isotope effects in synthetic carbonates. Geochim. Cosmochim. Acta 61, 3461–3475.
Kluge, T., Affek, H.P., 2012. Quantifying kinetic fractionation in Bunker Cave speleothems using Δ_{47}. Quat. Sci. Rev. 9, 2–4.
Landman, N.H., Cochran, J.K., Larson, N.L., Brezina, J., Garb, M.P., Harries, P.J., 2012. Methane seeps as ammonite habitats in the US Western Interior Seaway revealed by isotopic analyses of well-preserved shell material. Geology 40, 507–510.
Landman, N.H., Cochran, J.K., Rye, D.M., Tanabe, K., Arnold, J.M., 1994. Early life history of Nautilus: evidence from isotopic analyses of aquarium-reared species. Paleobiology 20, 40–51.
LeGrande, A.N., Schmidt, G.A., 2006. Global gridded data set of the oxygen isotopic composition in seawater. Geophys. Res. Lett. 33, L12604.
L'Homme, N., Clarke, G.K.C., 2005. Global budget of water isotopes inferred from polar ice sheets. Geophys. Res. Lett. 32, L20502.
Li, L.Q., Keller, G., 1999. Variability in Late Cretaceous climate and deep waters: evidence from stable isotopes. Mar. Geol. 161, 171–190.
MacLeod, K.G., Huber, B.T., Isaza-Londono, C., 2005. North Atlantic warming during global cooling at the end of the Cretaceous. Geology 33, 437–440.
Markwick, P.J., 1998. Fossil crocodilians as indicators of Late Cretaceous and Cenozoic climates: implications for using palaeontological data in reconstructing palaeoclimate. Palaeogeogr. Palaeoclimatol.Palaeoecol. 137, 205–271.
McConnaughey, T.A., 2003. Sub-equilibrium oxygen-18 and carbon-13 levels in biological carbonates: carbonate and kinetic models. Coral Reefs 22, 316–327.
McConnaughey, T.A., Gillikin, D.P., 2008. Carbon isotopes in mollusk shell carbonates. Geo-Mar. Lett. 28, 287–299.
McDonough, K.J., Cross, T.A., 1991. Late Cretaceous sea level from a Paleoshoreline. J. Geophys. Res. 96, 6591–6607.
Meckler, A.N., Adkins, J.F., Eiler, J.M., Cobb, K.M., 2009. Constraints from clumped isotope analyses of a stalagmite on maximum tropical temperature change through the late Pleistocene. Geochim. Cosmochim. Acta A863, A863.
Merritt, D.A., Hayes, J.M., 1994. Factors controlling precision and accuracy in isotope-ratio-monitoring mass-spectrometry. Anal. Chem. 66, 2336–2347.
Metz, C.L., 2010. Tectonic controls on the genesis and distribution of late Cretaceous, Western Interior Basin hydrocarbon-seep mounds (Tepee Buttes) of North America. J. Geol. 118, 201–213.
Miall, A.D., Catuneanu, O., Vakarelov, B.K., Post, R., Andrew, D.M., 2008. The Western Interior Basin, Sedimentary Basins of the World. Elsevier, pp. 329–362.
Oba, T., Kai, M., Tanabe, K., 1992. Early life-history of Nautilus pompilius inferred from oxygen isotope examinations. Mar. Biol. 113, 211–217.
Otto-Bliesner, B.L., Brady, E.C., Shields, C., 2002. Late Cretaceous ocean: coupled simulations with the national center for atmospheric research climate system model. J. Geophys. Res.–Atmos., 107.
Passey, B.H., Levin, N.E., Cerling, T.E., Brown, F.H., Eiler, J.M., 2010. High-temperature environments of human evolution in East Africa based on bond ordering in paleosol carbonates. Proc. Natl. Acad. Sci. USA 107, 11245–11249.
Poulsen, C.J., Barron, E.J., Peterson, W.H., Wilson, P.A., 1999. A reinterpretation of mid-Cretaceous shallow marine temperatures through model-data comparison. Paleoceanography 14, 679–697.
Rexfort, A., Mutterlose, J., 2006. Stable isotope records from Sepia officinalis–a key to understanding the ecology of belemnites? Earth Planet. Sci. Lett. 247, 212–221.
Rowley, D.B., Garzione, C.N., 2007. Stable isotope-based paleoaltimetry. Annu. Rev. Earth Planet. Sci. 35, 463–508.
Royer, D.L., Berner, R.A., Beerling, D.J., 2001. Phanerozoic atmospheric CO_2 change: evaluating geochemical and paleobiological approaches. Earth-Sci. Rev. 54, 349–392.
Rye, D.M., Sommer, M.A., 1980. Reconstructing Paleotemperatures and Paleosalinity Regimes with Oxygen Isotopes. In: Rhoads, D.C., Lutz, R.A. (Eds.), Skeletal Growh of Aquatic Organisms. Plenum Press, New York, pp. 169–202.
Schauble, E.A., Ghosh, P., Eiler, J.M., 2006. Preferential formation of $^{13}C^{18}O$ bonds in carbonate minerals, estimated using first-principles lattice dynamics. Geochim. Cosmochim. Acta 70, 2510–2529.
Schone, B.R., Tanabe, K., Dettman, D.L., Sato, S., 2003. Environmental controls on shell growth rates and $\delta^{18}O$ of the shallow-marine bivalve mollusk Phacosoma japonicum in Japan. Mar. Biol. 42,, 73–85.
Shackleton, N.J., Hall, M.A., Boersma, A., 1984. Oxygen and carbon isotope data from Leg 74 foraminifers. Initial Rep. Deep Sea Drilling Proj. 74, 599–612.
Shackleton, N.J., Kennett, J.P., 1975. Paleotemperature history of the Cenozoic and the initiation of Antarctica glaciation: oxygen and carbon isotopic analyses in DSDP Sites 277, 279, and 281. Initial Rep. Deep Sea Drilling Proj. 29, 743–755.
Shanahan, T.M., Pigati, J.S., Dettman, D.L., Quade, J., 2005. Isotopic variability in the aragonite shells of freshwater gastropods living in springs with nearly constant temperature and isotopic composition. Geochim. Cosmochim. Acta 69, 3949–3966.
Shields, G.A., Carden, G.A.F., Veizer, J., Meidla, T., Rong, J.Y., Li, R.Y., 2003. Sr, C, and O isotope geochemistry of Ordovician brachiopods: a major isotopic event around the Middle-Late Ordovician transition. Geochim. Cosmochim. Acta 67, 2005–2025.
Slingerland, R., Kump, L.R., Arthur, M.A., Fawcett, P.J., Sageman, B.B., Barron, E.J., 1996. Estuarine circulation in the Turonian Western Interior seaway of North America. Geol. Soc. Am. Bull. 108, 941–952.
Sloan, L.C., Barron, E.J., 1990. ''Equable'' climates during Earth history? Geology 18, 489–492.
Swart, P.K., Burns, S.J., Leder, J.J., 1991. Fractionation of the stable isotopes of oxygen and carbon in carbon-dioxide during the reaction of calcite with phosphoric-acid as a function of temperature and technique. Chem. Geol. 86, 89–96.
Thiagarajan, N., Adkins, J., Eiler, J., 2011. Carbonate clumped isotope thermometry of deep-sea corals and implications for vital effects. Geochim. Cosmochim. Acta 75, 4416–4425.
Tourtelot, H.A., Rye, R.O., 1969. Distribution of oxygen and carbon isotopes in fossils of late Cretaceous Age, Western Interior Region of North America. Geol. Soc. Am. Bull. 80, 1903–1922.
Tripati, A.K., Eagle, R.A., Thiagarajan, N., Gagnon, A.C., Bauch, H., Halloran, P.R., Eiler, J.M., 2010. $^{13}C^{18}O$ isotope signatures and 'clumped isotope' thermometry in foraminifera and coccoliths. Geochim. Cosmochim. Acta 74, 5697–5717.
Turekian, K.K., Armstrong, R.L., 1961. Chemical and Mineralogical Composition of Fossil Molluscan Shells from the Fox Hills Formation South Dakota. Geol. Soc. Am. Bull. 72, 1817–1828.
Ullmann, C.V., Wiechert, U., Korte, C., 2010. Oxygen isotope fluctuations in a modern North Sea oyster (Crassostrea gigas) compared with annual variations in seawater temperature: implications for palaeoclimate studies. Chem. Geol. 277, 160–166.
Upchurch, G.R., Wolfe, J.A., 1993. Cretaceous vegetation of the western interior and adjacent regions of North America. In: Caldwell, W.G.E., Kauffman, E.G. (Eds.), Evolution of the Western Interior Basin. Geological Association of Canada, pp. 243–281.
Urey, H.C., Lowenstam, H.A., Epstein, S., McKinney, C.R., 1951. Measurement of Paleotemperatures and temperatures of the Upper Cretaceous of England, Denmark, and the Southeastern United States. Bull. Geol. Soc. Am. 62, 399–416.
Waage, K.M., 1968. The type Fox Hills formation, Cretaceous (Maestrichtian), South Dakota: Part 1—Stratigraphy and Paleoenvironments. Peabody Mus. Nat. Hist. Bull. 27, 177.
Wang, Z.G., Schauble, E.A., Eiler, J.M., 2004. Equilibrium thermodynamics of multiply substituted isotopologues of molecular gases. Geochim. Cosmochim. Acta 68, 4779–4797.
Weidman, C.R., Jones, G.A., Kyger, 1994. The long-lived mollusc Arctica islandica: a new paleoceanographic tool for the reconstruction of bottom temperatures for the continental shelves of the northern North Atlantic Ocean. J. Geophys. Res. 99, 18305–18314.
Wright, E.K., 1987. Stratification and paleocirculation of the Late Cretaceous Western Interior Seaway of North America. Geol. Soc. Am. Bull. 99, 480–490.
Zachos, J.C., Stott, L.D., Lohmann, K.C., 1994. Evolution of early Cenozoic marine temperatures. Paleoceanography 9, 353–387.